Carbon 205 (2023) 236–252

Contents lists available at ScienceDirect

Carbon

journal homepage: www.elsevier.com/locate/carbon

Review article

Modulating heat transport inside CNT assemblies: Multi-level optimization and structural synergy

Yuxin Ouyang [a,1], Lin Qiu [a,*,1], Xiaohua Zhang [b], Yanhui Feng [a,*]

[a] School of Energy and Environmental Engineering, University of Science and Technology Beijing, Beijing, 100083, PR China
[b] Innovation Center for Textile Science and Technology, Donghua University, Shanghai 201620, PR China

ARTICLE INFO

Keywords:
Carbon nanotube
Thermal conductivity
Interfacial thermal conductance
Multi-level modulation
Structural synergy

ABSTRACT

Due to their ultra-high thermal conductivity, carbon nanotubes (CNTs) have become a hot spot for thermal enhancement materials. However, many researchers have found that the CNT assemblies had a reduced thermal conductivity by 2–3 orders of magnitude even though that of an individual CNT was 3700 W m^{-1} K^{-1}. From a nanoscale perspective, interfacial phonon scattering is widely accepted as the culprit for above-mentioned enormous reduction of thermal transport. This paper reviews the thermal transport mechanisms and their enhancement approaches using the modification of micro- and nano-scale guest materials. Various aspects like the individual-level to batch-level modulations of CNTs, the phonon transport law, the thermal enhancement effect and the different interface optimization mechanisms are summarized. The bonding force is the best way to improve the interfacial thermal transport, and the excellent spatial arrangement design of CNTs can greatly enhance the directional thermal transport. In addition, a multi-material structural synergy to break through the limitation of weak phonon transport under the van der Waals force is also discussed.

1. Introduction

The rapid development of micro- and nano-scale electronics has brought about a dramatic increase in high-power density and high-heat flux generation. At present, the heat flux density of advanced equipment (e.g. communications satellites, directed-energy weapons, and wide band gap semi-conductors) has reached hundreds of watts or even kilowatts in the core zone with square millimeter (e.g. The maximum core of the 12th generation Core is 7.67 m^2). There is an urgent need to design an effective thermal management strategy between the heat source region and cooling environment, to facilitate the quick transfer of the generated heat flux. Thermal interface materials (TIMs) can fulfill the commitment of dissipating the heat generated by heat source [1,2]. As a highly conductive material [3–8], carbon nanotubes (CNTs) can be assembled into thermally functional materials [9–11]. For example, CNTs are dense and can be oriented to assemble two-dimensional (2D) CNT films under temperature, catalyst, etc. [7], and 1D CNT fibers possess excellent axial heat transport ability [12]. However, simply assembled composites undermine the thermal superiority of the raw material without considering the effect of heat transfer across materials, and they further cannot meet the needs of thermal management in practical applications. The main reason for the huge decrease of the effective thermal conductivity (TC) of CNTs attributes to the phonon scattering at defects and interfaces. Influence of different controlling factors can lead to differences in the TC of the assembled materials, such as the enhancement effect of the quality, density and orientation uniformity of the CNTs in the array. It is required to summarize these relevant factors to identify the keys in thermally efficient and conductive materials.

This review has sorted out and summarized the researches around the thermal enhancement of CNTs assembles and composites and strategies on phonon transmission, CNTs modulation, and synergistic enhancement. The design ideas of different functionalized carbon nanotube assemblies are analyzed in terms of thermal mechanism, and the valuable references are summarized.

2. Phonon transmission and scattering theories across interface

In the past dozen years, most thermal characterizations (e.g. guarded hot plate [13], transient hot wire [14–18], T-type probe method [19–22], 3ω method [23–27] and laser flash technique [28–32] are based on Fourier-based thermal diffusion models which are suitable for macroscopic and mesoscopic heat transport analysis). (Fig. 1). The impact of phonon transmission and scattering in CNT assembly materials is only manifested by alteration of local thermal channel or global

* Corresponding authors.
E-mail addresses: qiulin111@sina.com (L. Qiu), yhfeng@me.ustb.edu.cn (Y. Feng).
[1] These authors contributed equally to this work.

https://doi.org/10.1016/j.carbon.2023.01.041
Received 5 November 2022; Received in revised form 21 December 2022; Accepted 19 January 2023
Available online 21 January 2023
0008-6223/

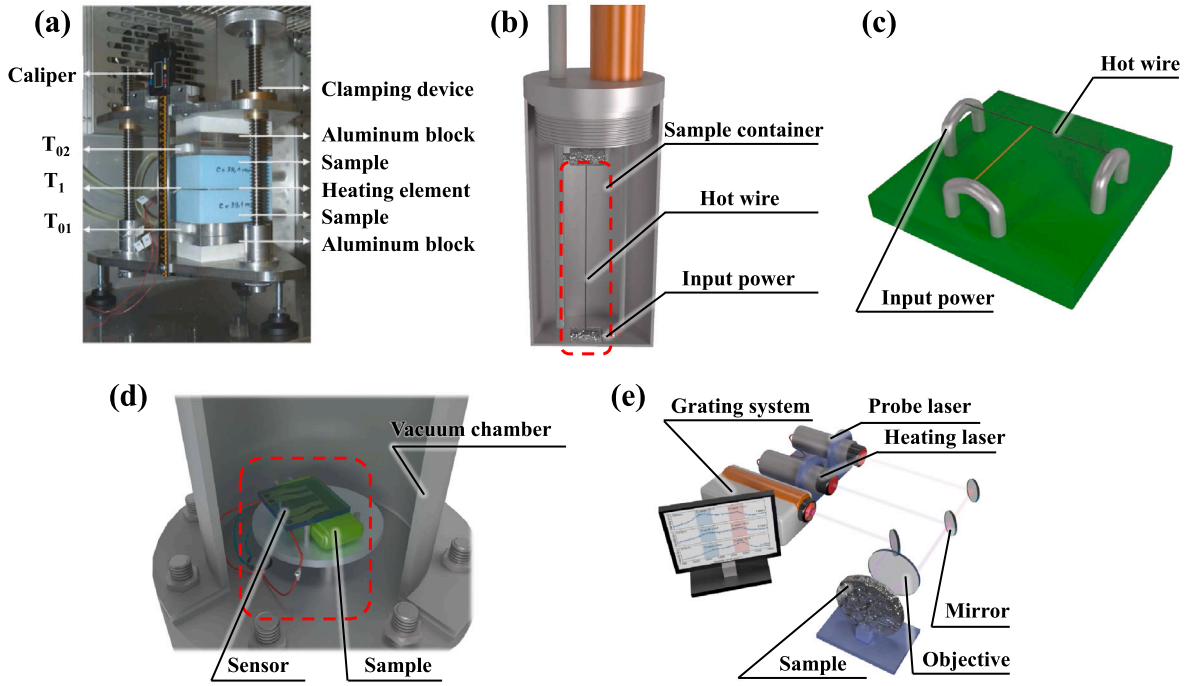

Fig. 1. Schematic diagram of thermophysical measuring methods, including (a) Guarded hot plate method, (b) Hot wire method, (c) T-type probe method, (d) 3ω method and (e) Laser flash method.
Source: Reprinted with permission from Ref. [33].

thermophysical parameters such as TC (κ) and thermal diffusivity (TD, α) under these characterizations. It can be seen in Fig. 2 that the difference of TC across the interface of materials can be ascribed to phonon scattering under the influence of a harmonic forces. As the key factor, Umklapp process affects the reciprocal lattice vector, resulting in the phonon momentum change and high interfacial thermal resistance (ITR, R_C).

In addition to scattering from collisions between phonons, phonon scattering also occurs at defects or crystal boundaries. The quantitative parameter of the resistance to heat transfer can be defined as ITR, or its reverse, interfacial thermal conductance (ITC, $G_C = 1/R_C$). Besides the theory of the effect of phonon transfer direction, this interfacial barrier is affected by a variety of factors, including: (i) the intrinsic properties of contacting materials, such as acoustic impedance and phonon density of states [34]; (ii) geometric defects on the interface (real versus apparent contact area) and (iii) the types of interfacial interaction (e.g. covalent bonding and van der Waals forces) [35]. In interfacial nanostructure, phonons are subject to additional constraints imposed by boundaries and interfaces, which causes the ITR and reduces the overall TC of the material in turn, as shown in Fig. 2 [36]. These structural barriers can be exhibited in molecular dynamics (MD), which analyzes the changes of interatomic and external forces on the spatial coordinates of particles based on the mechanical and displacement changes of atoms in the system. Thermophysical properties are calculated by utilizing statistical physics when system turns back to equilibrium. Based on the choice of the system's potential function, more complex polyatomic relationships can be further explored. For example, Lennard-Jones potentials for nonbonded interactions were presented for changing face-centered cubes [37–39], gas atoms [40,41] and non-bonded/bonded interaction [42,43].

Complex CNT structure is constrained by multiple interfacial interactions such as van der Waals forces, and the motion and frequency domain characteristics of phonons are also limited by those interactions. It is generally believed that the ITC is mainly affected by the phonon transmission probability at the interface, the phonon wave vector and mode and the group velocity [44]:

$$G = \frac{1}{2(2\pi)^3}\sum_i \int_{\boldsymbol{k}} \frac{1}{k_B} T^2 \alpha_{a\to b}(\boldsymbol{k},i) \times (\hbar\omega(\boldsymbol{k},i))^2 \, |V(\boldsymbol{k},i)\cdot \boldsymbol{n}| \times \frac{\exp(\hbar\omega(\boldsymbol{k},i)/k_B T)}{[\exp(\hbar\omega(\boldsymbol{k},i)/k_B T)-1]^2} d\boldsymbol{k} \quad (1)$$

where G denotes ITC, k_B is Boltzmann constant, $\boldsymbol{k}$ is the phonon wave vector, $\boldsymbol{n}$ is the unit vector in the direction of the interface longitudinal direction, $\alpha_{a\to b}$ is the averaged transmission coefficient of materials a to b, i is the phonon model, $\hbar$ is the reduced Planck's constant, $\omega(\boldsymbol{k},i)$ and $V(\boldsymbol{k},i)$ is the phonon frequency and group velocity corresponding to $\boldsymbol{k}$ and i, respectively.

G can be improved by increasing phonon modes i, phonon group velocity $V(\boldsymbol{k},i)$ and phonon transmission coefficient $\alpha_{a\to b}$. Usage of a force stronger than van der Waals force or exciting low-frequency phonons, are both effective ways to improve $V(\boldsymbol{k},i)$. The short functional groups (–CH_2–, –C_3H_6–, etc.) modified between adjacent CNTs can result in 8-fold improvement in G, which is sourced from the additional covalent bond to complement the limited binding effect from van der Waals forces [45]. The "surface relaxation effect" is proposed which suggests that the great excitation of the low-frequency phonon mode of occurs when the metal reaches the nanoscale. This is when the metal nanoparticles have abundant low-frequency phonon modes [46], and this can improve the interfacial thermal transport process. Similarly, the "electro-phonon coupling effect" of metals can redistribute the energy of phonons, which is beneficial to improving the interface phonon transmittance [47]. Based on phonon vibrational density of states (VDOS) analysis, the reduction of axial strain energy of CNTs can promote the blue shift of low-frequency phonon, thereby reducing the phonon scattering at the cross-tube interface (junction) improving ITC [48].

Besides the transmission limits (Eq. (1)), the acoustic mismatch model (AMM) and diffuse mismatch model (DMM) are also effective ways to evaluate the averaged transmission coefficient and ITC. AMM is

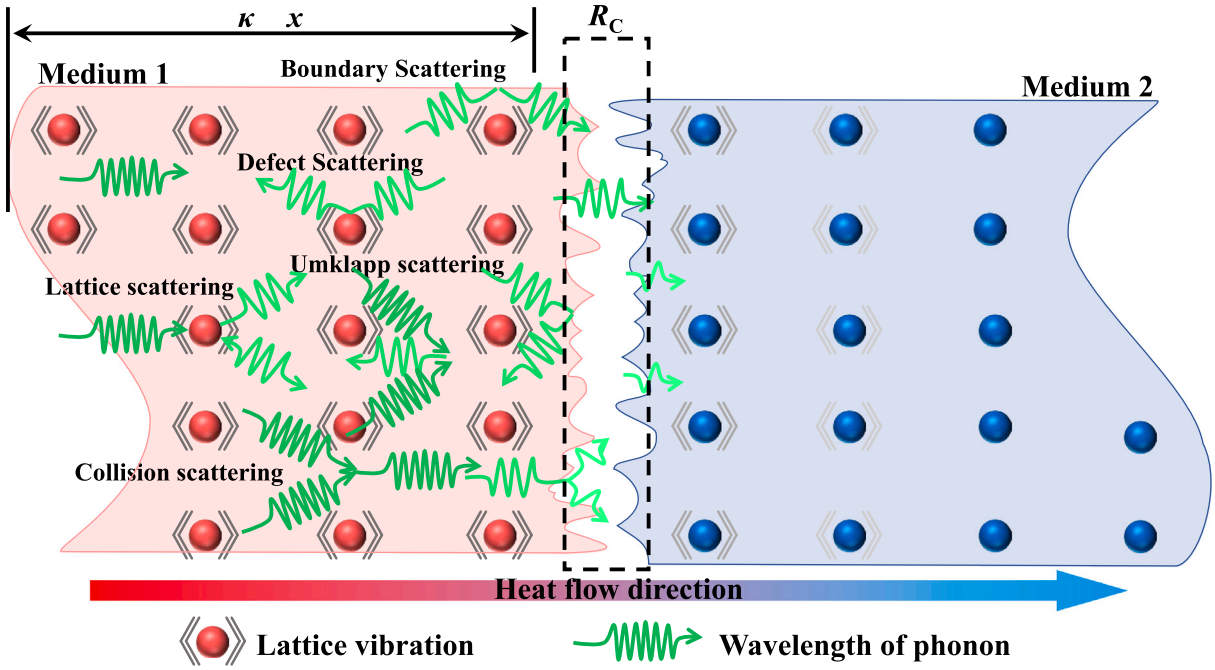

Fig. 2. Schematic diagram of various thermal processes, including the unidirectional phonon diffusion model under temperature difference ΔT and distance x, and the interfacial phonon scattering and generation of interfacial thermal resistance (ITR) R_C.

based on acoustic transmission and reflection between two linear elastic solids, it is most appropriate for calculating the experimental measurements below room temperature (RT) because this approach ignores the lattice [49,50]. The phonon spectrum is dominated by long-wavelength phonons, and the complicated transmissive or reflective mode (two longitudinal, four transverse) conversions are typically ignored, it can be shown as below:

$$\alpha_{a\to b} = \frac{4\frac{\rho_b V(\boldsymbol{k},b)}{\rho_a V(\boldsymbol{k},a)}\frac{\cos\theta(\boldsymbol{k},b)}{\cos\theta(\boldsymbol{k},a)}}{(\frac{\rho_b V(\boldsymbol{k},b)}{\rho_a V(\boldsymbol{k},a)} + \frac{\cos\theta(\boldsymbol{k},b)}{\cos\theta(\boldsymbol{k},a)})^2} \tag{2}$$

where ρ is density and θ is the direction and related to the acoustic analog of Snell's law, $\sin\theta(a)/V(a) = \sin\theta(b)/V(b)$.

DMM is based on the assumption that interfacial phonons are scattered randomly with the loss of orientation, polarization ($\boldsymbol{k}$) and material properties [51–53]. The only constant is their angular frequency ω, which makes the density of states in material a proportional to the probability of phonon. This postulate implies that the chances for phonon incident from material a to transmit to material b are the same as those from material b to be reflected at the interface, that is,

$$\alpha_{a\to b,\omega} = 1 - \alpha_{b\to a,\omega} \tag{3}$$

The above equation is specified purely by the bulk dispersion relations two surrounding materials. Thus, the averaged transmission coefficient can be calculated in Debye solids at $T \ll \min(\theta(\mathrm{D},a),\theta(\mathrm{D},b))$ by using,

$$\alpha_{a\to b} = \frac{\sum_{\boldsymbol{k}} V^{-2}(\boldsymbol{k},b)}{\sum_{\boldsymbol{k}} V^{-2}(\boldsymbol{k},a) + \sum_{\boldsymbol{k}} V^{-2}(\boldsymbol{k},b)} \tag{4}$$

Given that most phonons have short wavelengths comparable to atomic spacing and surface roughness at above 26.85 °C, DMM is thought more appropriate than the AMM at noncryogenic temperatures and for rough interfaces.

With the advancement of artificial intelligence technology, machine learning (ML) based stochastic methods have been applied to the study of CNT composites in recent years. ML collects sample data sets from experimental measurements and theoretical calculations, and the sample sets had finished the Cross-validate with Root mean square error as the judgment condition. ML for investigating the thermal transport of CNT composites includes Artificial neural networks, Decision trees, Random forest, Support vector machine and k-nearest neighbors [54–56]. However, due to the fact that the key interfacial parameters (e.g., interfacial contact area, tube spacing) are still unknown and their relations are unclear, most studies focus on the prediction of macroscopic TC of composites, especially those with CNT as the nanofiller for thermal enhancement [57–60]. The combination of MD and ML is helpful for investigating the thermal conductivity and interfacial thermal conductance at the micro-nano scale, and various interatomic force field involved in MD can provide better screening function for ML application. The MD-ML method has been realized in interatomic force field for the purpose of thermal conductivity prediction [61,62]. In the future, this method can provide a reliable and effective way to explore the interfacial thermal transport for various microscale materials.

3. Individual- and batch-level thermal modulation of carbon nanotubes

For CNT assembly materials, there are many factors influencing the heat transport of the assembly due to the geometric defects and the weak interatomic forces at the interface. Growth control of CNTs is an effective pathway to reduce structural defects, and interface modulation between tubes can enhance phonon modes across-tubes, which finally enhances the thermal transport of CNT assembly.

3.1. Structural effect on thermal transport for an individual carbon nanotube

Hexagonal arrangement between carbon atoms and coaxial circular tube structure with more than a single layer brings about oriented thermal transport within CNTs, the ultra-high thermal conductance comes from the positive relation of lattice vibration and internal phonon mean free path (Fig. 2). The MD simulation found that the decrease in TC of CNTs is caused by the shortened free path, and the Umklapp scattering phenomenon played a pivotal role during these changes [3]. According measurement results of thermoelectric method or T-type method [4–6,21], Umklapp scatting process increases with the increasing temperature until 46.85–76.85 °C. However, with subsequent increase in

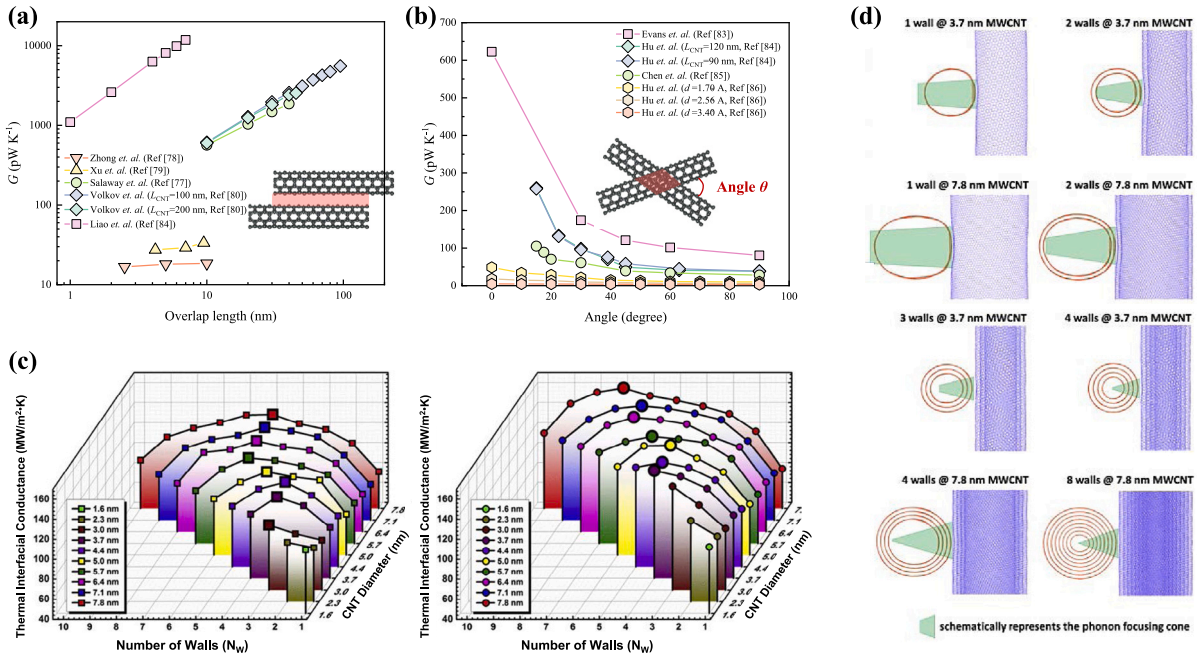

Fig. 3. The effect of contact area on the ITC across-tube: (a) Comparison of parallel CNT-CNT with different overlapping lengths, (b) Comparison of contact junction with different crossing angles, (c) Comparison of CNT wall number and outermost diameter, (d) Schematic diagram of the phonon focusing cone at cross-contact (90°) MWCNT junction.
Source: Reprinted with permission from Ref. [63] (Copyright (2017) Elsevier).

temperature, the process is inhibited, which will exponentially affect the CNT assemblies.

The nanostructure has an important influence on the TC of CNT and its composites. The number of tube walls is also one of the key factors that affects the change of diameter. The interactions of phonons and electrons between walls have great effect on the total TC of multi-walls carbon nanotubes (MWCNTs) [21], The wall perimeter is negatively correlated with TC for single-walled carbon nanotubes (SWCNTs). For a CNT with 1 nm diameter, the ITC is very close to the maximum possible value of the ballistic thermal conductance [4]. In a marked contrast, the interfacial contacts is not good for phonon propagation for CNTs with 2 or 3 nm diameters, smaller thermal conductance is observed due to the Umklapp process at high temperatures. For larger-scale CNT assemblies, although the diameter is correlated with the TC, the inter-tube interface occupies a larger proportion of the thermal impedance. TC of the pristine fibers decreased with increasing diameter from 30 ± 8 W m^{-1} K^{-1} (37 μm diameter) to 15 ± 2 W m^{-1} K^{-1} (60 μm diameter) [64]. Similar tendency has been observed in SWCNT fibers where TC increases from 5 W m^{-1} K^{-1} to 19 W m^{-1} K^{-1} as with 50% reduction in diameter. However, as the diameter is further reduced, the TC decreases to 17 W m^{-1} K^{-1}, owing to the thermal contact resistance between bundles [8].

Similar to electrical conductivity, TC has a positive correlation effect with nanotube length (L). Generally, the TC of a CNT increases with the length as the interface count reduces. Specifically, it is found that the TC is an exponential function of length for the CNTs, that is, $\kappa = L^{\beta}$, where β is related to the structure of CNT [65]. For example, $\beta = 0.4$ is found in (5,5) armchair SWCNT at room temperature based on MD simulation [66] and $\beta = 0.6 - 0.8$ are found in MWCNTs according to experimental measurements [67]. The length dependence of apparent TC (κ_{ap}) and apparent TD (α_{ap}) are quadratic functions for CNTs fibers [68,69], which can be expressed by $\kappa_{ap} = \kappa_{int} + a_{ra}L^2$ and $\alpha_{ap} = \alpha_{int} + b_{ra}L^2$, where κ_{int} and α_{int} denote the intrinsic TC and TD, respectively, a_{ra} and b_{ra} are constants related to radiative heat loss. The CNTs-added polymer composites were also shown this effect [69]. Apart from fiber-type materials, the negatively correlated improvement effect appears in CNTs arrays with the growth height at 10, 50, 80, 200 μm [70], the result is different from the conclusion in previous researches [71–73]. There has been no vibrant correlation between array height and ITC as the effects from other parameters isolated were difficult like diameter and density. According to the above studies, the quality of CNTs is the premise to ensure good thermal conduction in composites. However, the different phonon modes induced by the complex structure and the interfacial effect between nanotubes make it difficult to reveal the thermal properties of the assembled material.

3.2. Across-tube contact effect

In CNT fibers, arrays, networks, the nanotubes interact via van der Waals forces and entangle locally. The weak interaction force and the random assembly negatively alter the initial contact area and spacing between the tubes, and the degree of phonon scattering is much greater than the cause of the CNTs' own defects.

Due to the existence of defects and impurities (usually catalysts for CNTs growth) and the low density of CNTs assembly, the inter-tube ITC dominates the heat conduction in CNTs composites [74,75]. Atomistic Green's function [76,77] was used to calculate inter-tube ITR, which was much larger than the theoretical predication and greatly hindered the thermal transport in MWCNT bundles [74]. This section reviews the effect of contact area, interaction strength and the effects of the spatial arrangement on thermal transport of CNT assemblies.

3.3. Contact area across nanotubes

The contact area between adjacent nanotubes is a crucial parameter which embodies the range of inter-tube van der Waals forces and bonding. It is difficult to obtain the heat transfer across nanotubes directly from experimental data, MD simulation can provide a more intuitive expression of the impact of the contact area. Subsequently, the effect of contact area on crossing CNT-CNT structures and parallel CNT-CNT structures (crossing angle is 0°) have also been analyzed.

The overlapping length of parallel CNT-CNTs (axial contact length) is the main factor that affects the variation of the contact area [80–84]. The total ITC between tubes (G) shows a linear dependence on the overlap length (Fig. 3(a)), which attributes the improving total

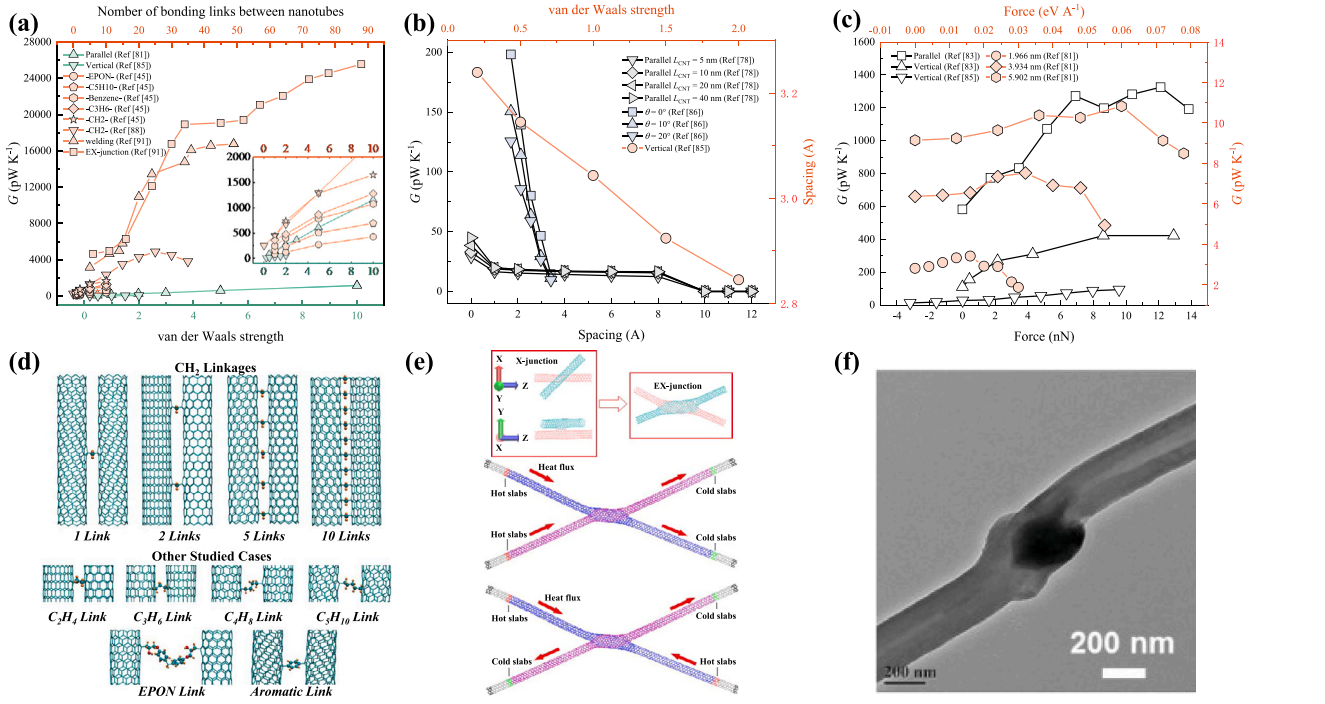

Fig. 4. Effect of inter-tube interaction strength and spacing on ITC, (a) Evolution of ITC versus van der Waals interaction, organic bonding links, and welding bonding, (b) Correlation between van der Waals strength and inter-tube spacing, and the effect of spacing on conductance under the different tube lengths and crossing angles, (c) The influence of external force on the ITC between nanotubes, (d) Schematic of organic links built between CNTs, (e) Schematic X-junction and EX-junction under weld bonding for CNTs, (f) Transmission electron microscope image for covalent bonded junction at CNT ends.
Source: Reprinted with permission from Ref. [45] (Copyright (2010) American Chemical Society), Ref. [78] (Copyright (2014) Elsevier), Ref. [79] (Copyright (2016) Elsevier).

strength of the interatomic force with the contact area increases. To cancel the effect of overlap length, the normalized interfacial thermal conductance (G_n, $W\,m^{-1}\,K^{-1}$) is generally used for discussion. Some studies corroborate that there is a slight downward trend for G_n with the increase of the overlap length [80–82], but another study [83] shows that G_n is independent of the overlap length. Therefore, it is believed that the interatomic force density on the parallel CNT-CNT contact area is not greatly affected by the increase of the overlap length.

When the intersection angle of adjacent contact CNTs changes from 0° to 90°, the area of its junction position changes correspondingly. Fig. 3(b) presents the evolution of G as a function of crossing angle in previous studies [85–88]. The relationship between the contact area and the intersection angle is $A = D^2/\sin(\theta)$, where A is the contact area, D is the diameter and θ is the crossing angle. When the angle increases, the effective contact area of the junction decreases, resulting in a significant drop in G. The experimental values of the crossed (10,10), (6,6), (5,5) MWCNT-MWCNTs with diameters of 74 nm and 112 nm are $\sim 10^4$ $pW\,K^{-1}$ [89], which is much higher than the simulation results [85–88]. The diameter and the force are main reasons for the complexity in comparing the experimental measurement and the simulation calculation well.

Attributed to the influence of diameter and wall number on interfacial phonons at cross-contact of 90°, there is a "focusing effect" of phonon transport in the radial direction of MWCNTs (Fig. 3(c) and (d)) [63,90], which is similar to transport in the cross-sectional direction of multilayer graphite [91]. The contact area at inter-tube should not be affected by the curvature for CNTs with a smaller number of walls which widens the area of phonon transmission. Although more phonons are thermalized as the number of walls increases, the enhancement in the tube strength leads to a decrease in the curvature. This eventually results in non-monotonic behavior of thermal conductance concerning the number of walls (Fig. 3(c)) [92].

3.3.1. Inter-tube interaction strength

In addition to expanding the range of inter-tube interactions, enhancing the strength of inter-tube interactions is also an effective method to boost ITC. For the van der Waals forces forming the basis of the CNT-CNT structure, the enhancement of its strength can further enhance the ITC [84,87]. Fig. 4(a) shows the evaluation of G versus the van der Waals strength. The parallel CNT-CNT structure ((10,10), L_{CNT} = 10 nm) has larger G than the vertical CNT-CNT ((10,10), L_{CNT} = 10 nm), but the improvement of both these characteristics is not much different under the same strength change (from 0.5 to 2) (parallel: 2.2 times boost, vertical: 2.5 times boost).

Due to the enhancement of the van der Waals strength between the tubes, the separation spacing between them is shortened (Fig. 4 (b)) [87]. In other words, when the spacing is reduced, apart from the enhancement of the interfacial interaction force, the interacting area between the tubes is further increased, so the G is further enhanced under the dual action [81,88]. As shown in Fig. 4(b), the increasing spacing weakens the advantage of larger contact area of the parallel CNT-CNT structure compared to the crossing CNT-CNT structure [81].

Although it is difficult to directly adjust the intensity of van der Waals force in actual situation, it is possible to apply external force across-tubes through certain post-processing methods. Fig. 4(c) shows the variation of the cross-tube G under the action of radial and axial external forces [84,85,87]. Similar to the trend in Fig. 4(b), the radial pressure assistances to reduce the inter-tube spacing and increase the contact area due to tube deformation, thereby boosting the ITC. However, the enhancement is different under different crossing angles. For vertical CNT-CNT, the tube deformation has a certain limit, and the enhancement becomes insignificant with the increase of pressure [85, 87]. For parallel CNT-CNT, severe tube deformation leads to the spatial displacement of the tubes and positional contact with larger curvature, which counteracts the increasing G [85].

When the parallel CNT-CNT is subjected to an external axial pulling force, the thermal resistance value between the tubes will also change. A study of the pull-down force effect on different overlap lengths is presented in Fig. 4(c) [84]. The effect of this force is twofold: (1) The increasing force reduces the inter-tube spacing and overlapping area before the axial tension approaches the fracture limit. Combined with

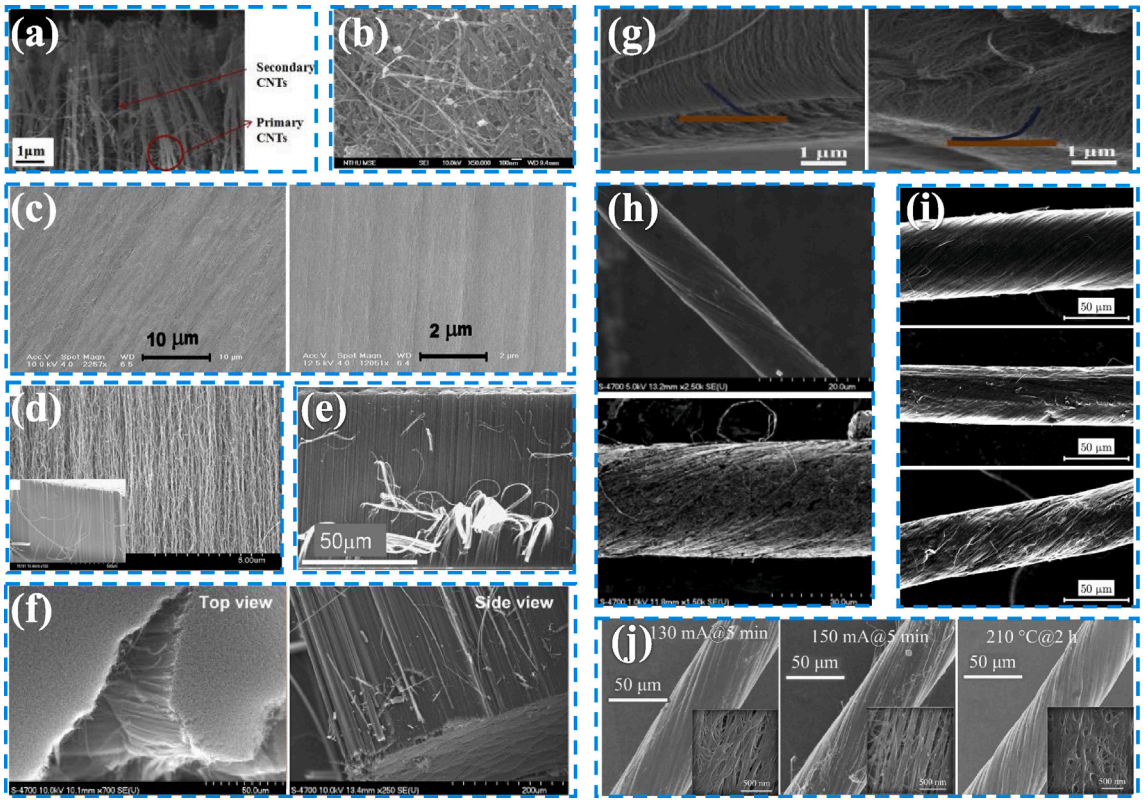

Fig. 5. Various carbon nanotube assemblies via growth control, (a) Purified SWCNT buckypaper, (b) Three-dimensional nanotube structures based on arrays and secondary branch, (c) Buckypaper under high ordering and high density, (d) Aligned CNTs on quartz substrate and (e) Vertically aligned MWCNT arrays grown via low-pressure CVD, (f) High-density (top) and low-density (bottom) CNT arrays at their root ends, (g) Vertically aligned MWCNT arrays up to ~6 mm high, (h) MWCNT fiber, (i) The pristine fibers of annealing treatment at three temperatures, (j) Bismaleimide composite fibers based on electrocuring.
Source: Reprinted with permission from Ref. [93] (Copyright (2018) Elsevier), Ref. [94] (Copyright (2008) Elsevier), Ref. [95] (Copyright (2013) Nature), Ref. [96] (Copyright (2007) Elsevier), Ref. [97] (Copyright (2006) American Institute of Physics), Ref. [98] (Copyright (2010) Elsevier), Ref. [99] (Copyright (2018) Elsevier), Ref. [100] (Copyright (2012) Elsevier), Ref. [64] (Copyright (2016) Elsevier), Ref. [11] (Copyright (2019) Elsevier).

the study of Fig. 4 (b) [81], it can be understood that the change of spacing is dominant among interface enhancing factors, which makes the effect of pulling force positive. (2) When the axial tension is close to the fracture limit, the interaction between the tubes is destroyed, the phonon scattering is further relieved, and G drops under the force.

Even though improving the contact area and spacing contributes to the enhancement of van der Waals forces at the interface, there is still a limit to the strength of the van der Waals force itself. To break through the limitation and achieve stronger interfacial interaction of CNT-CNT, an effective strategy is to build atomic bonding.

The interfacial carbon atoms are connected by utilizing electron beam/ion irradiation, mechanical manipulation with atomic force microscope, nanotube soldering, chemical functionalization, and heat welding, in order to achieve covalent bonded junction formation [78,101–105]. Using covalent bonds to connect carbon atoms between tubes can achieve orders of magnitude improvement according to theoretical simulations (Figs. 3(a) and 4(a)). It is difficult for organic links bonding to completely replace the van der Waals interaction. Moreover, a single bonding link is not enough to compensate for the weak interaction effect of van der Waals force [45]. Increasing the number of links at the interface is an effective means to improve the ITC. Increasing the overlapping length can increase the number of bonding links, and thus boost the ITC (Fig. 3(a)). In addition, the covalent bonding formed by welding method (Fig. 4(e)) can remarkably improve the ITC compared with the organic bonding links (Fig. 4(a)). Nearly 43-fold improvement in ITC comes from more covalent bonds between carbon atoms of two tubes [78,106,107]. Once ends of the randomly arranged CNTs are welded (Fig. 4(f)), the TC of the assembly can be boosted by 6-fold, which is close to the alignment [79].

3.3.2. *Complex coupling effect of spatial location*

In the random networks, cross-tube contact under van der Waals interaction brings about phonon interference [108,109]. Besides the contact area, spacing and interaction strength, the spatial location of the junctions also plays a key role in heat transport. According to the MD simulation [110], the increasing inter-junction distance reduced the number of scattering sites and thus improved TC in the random networks. The ultralow density network structures with 20 nm inter-junction distance [111] is 10-fold improvement in ITC compared with that with ~2 nm inter-junction distance [108].

Besides junctions, the thermophysical properties of CNT networks also strongly depends on the structure. The number of nanotube orientations determines the overall heat flux of the structure [110], which was similarly demonstrated in many researches [93,112,113]. The three-dimensional (3D) network structure was based on the vertically aligned CNT (VACNT) array, then the catalysts were used to generate secondary branches to increase the channels for heat dissipation (Fig. 5(a)). Reducing the density of growing primary VACNT arrays, the secondary branch increases the overall TC by approximately ~30 times. But with further increase in density, TC instead decreases, which is in line with the conclusion that phonon interference is enhanced [93,112]. The length of the CNTs in the network also affects the overall and in-plane TC. According to the research results from Volkov et al. [114], there is a secondary dependence of the fiber length on the electrical/thermal properties in the 3D CNT networks. When the dimension of the network drops to two magnitudes, the dependence turns out into a quadratic rule.

Table 1
Oriented thermal enhancement effect under growth control in CNT assembles.

Research team	Preparation	TC ($W m^{-1} K^{-1}$)	TD (10^{-4} m^2/s)	ITC ($W m^{-2} K^{-1}$)
Buckypaper				
Yue et al. [115]	Primary	1.19–2.92	\	\
Hong et al. [94]	Acid treatment	2.43–3.44	\	\
Gonnet et al. [116]	Magnetic alignment	42	\	\
Zhang et al. [95]	Post-processing array	370	\	\
Array				
Shaikh et al. [96]	Carbon vapor deposition 800 °C, H_2/Ar	8.3	\	\
Jakubinek et al. [117]	CVD 750 °C, Ar	~1	\	~10^5
Tong et al. [73]	Thermal CVD 750 °C	~250	\	~10^6
Cola et al. [118]	PECVD	\	0.4–2.8	~10^5
Bauer et al. [119]	CVD, 750 °C Ar/$H_2$0 (0 sccm) H_2/Ar (400→0 sccm)	49	\	\
	CVD 750 °C Ar/$H_2$0 (100 sccm) H_2/Ar (400→0 sccm)	64	\	\
	CVD 750 °C Ar/$H_2$0 (200 sccm) H_2/Ar (400→0 sccm)	62	\	\
	CVD 750 °C Ar/$H_2$0 (400 sccm) H_2/Ar (400→0 sccm)	55	\	\
	CVD 750 °C Ar/$H_2$0 (600 sccm) H_2/Ar (400→0 sccm)	58	\	\
	CVD 750 °C Ar/$H_2$0 (800 sccm) H_2/Ar (400→0 sccm)	69	\	\
	CVD 750 °C Ar/$H_2$0 (200 sccm) H_2/Ar (800→800 sccm)	74	\	\
	CVD 750 °C Ar/$H_2$0 (200 sccm) H_2/Ar (1200→1200 sccm)	79	\	\
Ivanov et al. [97]	CVD	6.4 ± 0.8	0.9 ± 0.1	\
		5.7 ± 0.7	0.011 ± 0.001–0.8 ± 0.2	\
	CVD Annealed in Ar at 2800 °C	3 ± 0.4	0.42 ± 0.06–2.1 ± 0.2	\
Fiber&bundle				
Jakubinek et al. [100]	Spun, water-assisted CVD	60 ± 20	\	\
Niven et al. [64]	Annealing at 2300 °C	60	\	\
	Annealing at 2700 °C	72–90	\	\
Qiu et al. [11]	Bismaleimide & curing	~177 ± 14	\	\

3.4. Alignment effect on interfacial thermal transport for carbon nanotube assemblies

For the application of oriented thermal transport, the arrangement design of CNTs in the assembled material needs to be considered. To maximize the in-plane thermal transport enhancement, the alignment of CNTs within the network needs to be considered. Taking buckypaper (Fig. 5(b)) as an example, random arrangement and surface defects of nanotubes lead to shorter phonon propagation length and lower ITC [94,115,120]. The inter-tube ITC were calculated to be within the range of 10–100 $pW K^{-1}$, which is much lower than the value of CNT under the theoretical length (421–8730 $pW K^{-1}$), that limited the in-plane TC remain 1.19–2.92 $W m^{-1} K^{-1}$ [115]. Similar results were also noticed in the SWCNT and MWCNT buckypaper, that is 2.43 and 3.44 $W m^{-1} K^{-1}$, respectively. The orientation of the SWCNTs in the buckypaper is improved by the magnetic field modulation method, which indicates that the in-plane TC reaches 42 $W m^{-1} K^{-1}$ and the anisotropy in-plane to out-of-plane ratio reaches a maximum of 3.5 [116]. High temperature and pressure treatment of CNT buckypaper also increased its ITC from 1.2 to 14.5 $W K^{-1}$, while the in-plane and cross-plane TC was increased by 1.41 and 1.44 times, respectively [94]. When the nanotubes within the buckypaper network achieve high ordering and high density (Fig. 5(c)), their in-plane TC can be as high as 370 $W m^{-1} K^{-1}$, while the anisotropy ratio is ~2.5 [95].

The CNT arrays are grown and arranged as CNTs in a certain direction so that normal heat flow predominates the heat transfer. Growth control on CNT array is using the widely-adopted longitudinal thermal enhancement strategy, which is usually based on the regulation of preparation including modifying chemical vapor deposition (CVD) to plasma-enhanced CVD (PECVD), or changing catalyst and growing environment (i.e., temperature, and atmosphere). Table 1 shows representative research results that focused on the exploration of catalyst (i.e., type, content and layer thickness), carbon source (i.e., type, and flow rate) and environmental treatment (i.e., temperature, gas ratio, and annealing parameters). The TC of the array decreases with the increasing height, due to the increased defect density in higher arrays (Fig. 5(d)) [96]. A series of preparation were used to reduce tube spacing within an array, which can improve heat conduction capability. The addition of ferrocene catalyst could affect the shape, inner diameter and outer diameter of the CNT. Increasing the inner diameters can decrease the density of all array [119]. Furthermore, the addition of water enhanced the longitudinal TC and increased the hydrogen content in the growth environment also further improved it. It is reported that the 200 sccm Ar/$H_2$0 and 1200 sccm H_2/Ar can result in the 1.6-fold improvement in TC of the array.

Similarly, the array can boost TC to 10–15 $W m^{-1} K^{-1}$ after annealing treatment in Ar atmosphere at 2800 °C [97], owing to the fact that more crystalline, straight and dense CNTs grow under that

condition (Fig. 5(e)). Cleaner sidewalls, fewer sidewall defects and continuity at junctions of CNT segments with different diameters were corroborated by multiple methods. In addition, the uniformity of CNT diameter also has a positive effect on the improvement of the ITC. The high density of CNT array leads to larger surface contact area (Fig. 5(f)) [98,117], and thus increasing the ITC. The increasing height of the CNT array bring about the decreasing ITC due to more defects and amorphous carbon in the tall array. When the thickness of catalyst layer (2-−11 nm) and the flow rate of carbon source (100–300 sccm) were controlled, high quality arrays with ~25 × 10^4 W m^{-2} K^{-1} (the ITC per unit area) were produced, which is 1.2 times higher than commercial silver epoxy after curing (Fig. 5(g)) [99]. CNT fibers were drawn and entangled from the array and they possessed high orientation along the axial direction [121,122]. Table 1 summarizes the most representative research outcomes. MWCNTs fiber (Fig. 5(h)) was spun from vertically aligned MWCNT arrays with 10 μm diameter and ~60–80 mm length, which is grown by water-assisted CVD. Its TC at RT was improved to 60 ± 20 W m^{-1} K^{-1} [100]. The annealing process at 2300 °C and 2700 °C increased TC (26.85 °C) by ~200% and 240%–300% (Fig. 5(i)), respectively [64]. Electro-curing scheme using bismaleimide (BMI) formed oriented cross-linking of BMI at inter-tube interfaces with CNT fibers (Fig. 5 (j)), brought about a remarkable TC improvement from 30 ± 3.6 W m^{-1} K^{-1} to 177 ± 14 W m^{-1} K^{-1} [11].

This section evaluates individual- and batch-CNT modulation studies to mitigate the disadvantage of reduced TC of CNT assemblies. Among them, improving the weak interfacial force between nanotubes is the most effective way to enhance the overall TC, and enhancing the ordering of CNTs can achieve efficient oriented thermal transport.

4. Thermal enhancement strategies

It is a strategy to preferentially retain the highly thermal conductive advantage of CNTs themselves via tuning the structure and interface of CNTs in assembly to enhance the overall thermal transport effect. However, when the composite material is a complex network structure [109,123], these strategies have the drawbacks like complicated process and insignificant improvement effect [109,124]. By introducing other thermally synergistic materials, the unsatisfactory thermal transport of pure CNT assembled materials is improved. Under the action of structural synergy, the TC of the composite material is further enhanced.

4.1. Phonon resonance mechanism for across-tube interfaces

Interfacial phonon scattering mainly arises from the longer phonon propagation length and CNT surficial defects. Van der Waals forces between tubes still have limitations, and bonding strategy is unable to fully cover the assemblies composed of a large number of CNTs [125]. In order to improve the weak coupling of interface, the use of resonant coupling is an effective strategy in engineering. The manipulation of phonon coherence helps to excite the energy carrier density [126], which can achieve effective across-interface thermal transport. The hybridized phonon modes, phonon localization and modal phonon interference are the main indicators of phonon coherence for resonant coupling in a large number of studies [127,128].

Low-frequency phonon resonant coupling between nanotubes is an effective thermal enhancement strategy that can be applied to large-scale CNT assemblies. Resonant coupling can be achieved by a variety of methods, including optical pulse [129–131], heat pulse [132,133], hammer impact [134], friction [135,136], and additive modification [137–139]. Optical pulse and heat pulse drive coherent atomic motion between nanotubes, whereas the radial and axial vibration modes (e.g. radial breathing mode, G mode) are excited and exchanged by pulses, where the radial modes produce strong and long-term coupling effects. The radial and axial mechanical interference (hammer impact and friction) affects the inter-tube spacing and excites different phonon modes/coupling forms, but the phonon resonance is hardly maintained after removing the interference. Additive modification is based on structural synergies across scales, the nano-enhancer fills the interface of tubes and induces stronger phonon transmission, which induces the low-frequency resonance of inter-tube atoms and thus enhances the thermal transport. Meanwhile, the modified composites are able to give a stable maintenance for the enhanced TC in the application. Therefore, it is an effective strategy to introduce nanoparticles and polymer chains, to enhance the phonon resonance of interfacial carbon atoms to broaden thermal transport channels.

The optimization effect of nano-carbon and metal nanoparticles can build a continuous thermal network, facilitating efficient heat transfer [140]. The electron exchange-transfer mechanism was notified in two noble metal nanoparticles (palladium and platinum) and carbon atoms, thereby increasing the interaction and thermal transport channels at the interface [137]. The loading of gold nanoparticles (Fig. 6(a)) boosted the G value between the tube bundles (12.5 μm diameter) by a 1.7-fold improvement (corresponding to the highest TC of the fiber is 52 W m^{-1} K^{-1}), the mechanism is sourced from increased phonon vibrational density and low frequency phonon excitation, which increases the distance of the phonon transport [141]. Through the aggregation of pre-functionalized silver nanoparticles on MWCNTs, the phonon transport junctions were generated in assembled TIMs and improved TC to 160 W m^{-1} K^{-1}, which reduced the temperature difference of the central processing unit device and heat sink from 15.6 °C to 13.5 °C [142]. The alignment behavior of CNTs under a magnetic field can trigger the TC percolation effect and obtained a significant improvement in the thermal transport of phonons at the CNT-Fe_3O_4 interface [138].

Non-metallic nanomaterials and physical/chemical modification at the interface can further created new heat transfer channels, which enhances the heat conduction. It is corroborated that iodine chains can improve the TC with 1.55-fold improvement (corresponding to the highest TC that is 47.3 W m^{-1} K^{-1}) on CNT fiber (Fig. 6 (b)) [69]. Furthermore, strong acid and iodine chains can be utilized to modify the cross-tube interfaces. Functional groups such as hydroxyl, carboxyl, and amide groups from acid (Fig. 6(c)) could effectively improve the ITC between CNTs [139]. The interface was physicochemically modified with linkers to obtain TC as high as 635 W m^{-1} K^{-1} [12]. The physical densification of CNTs and the deposition of carbonaceous coatings improved the ITC, and the in-plane oriented films weaved via CNT microfibers obtained an extremely high TC of nearly 770 W m^{-1} K^{-1} [143]. Local densification and acidification were carried out on the interface between tubes, the electrostatic adsorption force and short functional groups (–OH, –CH_2–, –CH_3, –C=O, which can be seen in Fig. 6(d)) were successfully introduced into the interface in fibers (12.5 μm diameter). Based on the above two types of force stronger than the van der Waals force, TC achieved a nearly 2.4-fold improvement (corresponding to the highest of the fiber 50.5 W m^{-1} K^{-1}) [68]. Assigning soft long-chain polymers such as polyurethane and polyethylene to the groove sites of the contacting CNTs, the excited phonons lead to a low-frequency resonance mechanism across the tube positions, which improved significantly the inter-tube ITC by 79 % [144]. Among them, the long-chain polyethylene molecular chain placed in the grooves on both sides of the two parallel CNTs served as a thermal switch knob(Fig. 6(e)). When the relative angle of the chains become flattened compared with the direction of the CNT axis (30–60°), the CNT contacts related to the phonon coupling is strongly enhanced, and thus the ITC is increased by ~120% [145].

4.2. Synergistic thermal conduction network of multiple materials

The addition of some nanomaterials helps to optimize the atomic forces between CNT tubes. Thermal conduction networks are built via the interaction of polyatomic systems when the dimensions of other thermally conductive materials in the composite are greater than

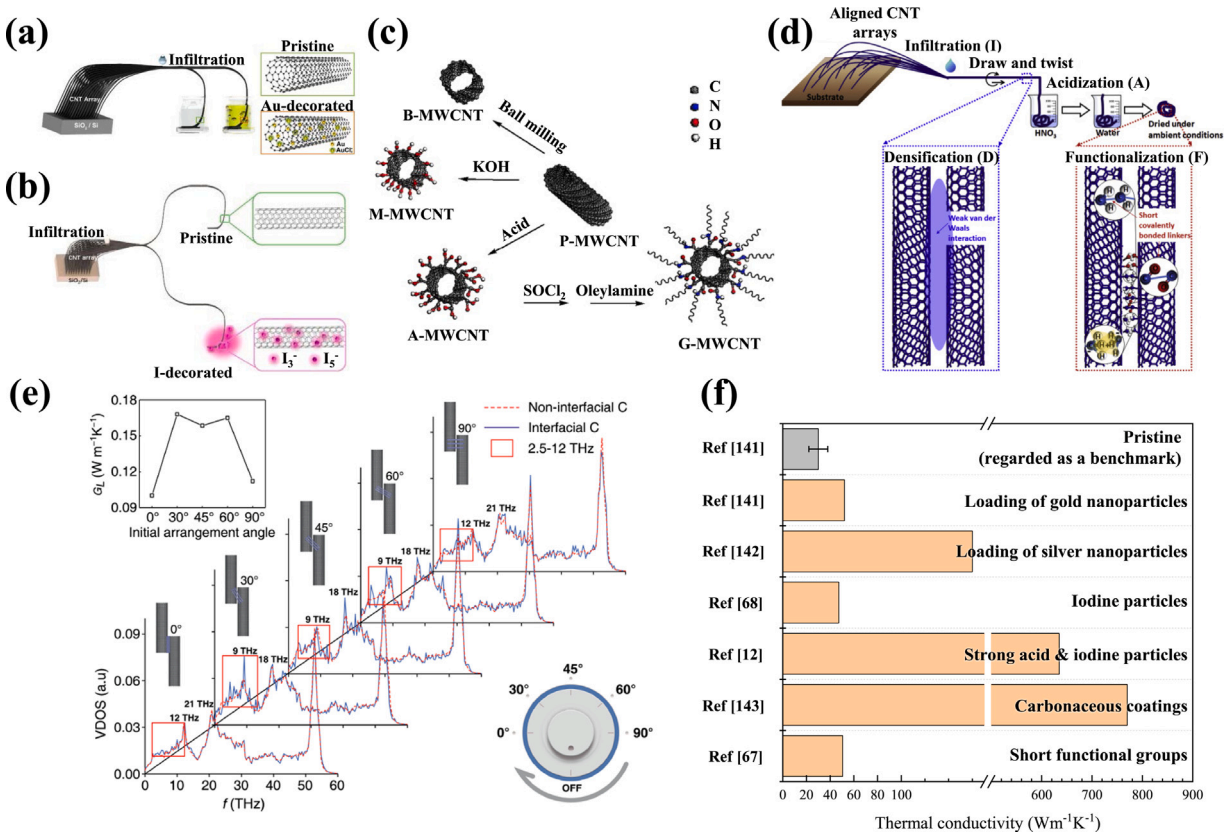

Fig. 6. Example of interface low-frequency phonon coupling (a) The preparation process of gold nanoparticles/CNT fibers by dipping into a 10 mL $HAuCl_4 \cdot 4H_2O$ solution for 1 h to introduce the gold nanoparticles, (b) The preparation process of iodine-decorated CNT fibers with exposing to iodine vapor for 30 min, (c) Schematic processes of the chemical and mechanical treatments to introduce hydroxyl groups, carboxylic groups, and amidocyanogen, (d) Two-stage manipulations on functionalized CNT fibers: at the first-stage, the fiber inner tube spacing is densified by physical penetration, stretching and twisting; at the second-stage, covalent bonding at the interface via chemical acidification and short functional groups, (e) Variation of the resonance frequency of polyethylene molecular chains at different inclination angles along the parallel CNT axis, (f) TC comparison of materials assembled by modified composite CNT fibers.
Source: Reprinted with permission from Ref. [141] (Copyright (2019) Elsevier), Ref. [69] (Copyright (2018) Elsevier), Ref. [139] (Copyright (2010) Elsevier), Ref. [68] (Copyright (2016) Elsevier), Ref. [145] (Copyright (2022) Elsevier).

or equal to CNTs. Because graphene nanoplatelets (GNPs) have low-dimensional structural features and advantages of physical properties, they can further optimize the performance of CNT networks, and form new thermal conductive assemblies to achieve synergistic enhancement [146–149]. In terms of structure, GNPs can act as bridges in the CNT network (Fig. 7(a)). This reduces the aggregation due to the intertwining of 1D nanotubes and thus enhances the overall dispersion. With longer nanotubes and optimal filler ratios, the coverage of the network was further increased, resulting in a 1.48-fold enhancement in TC, along with synergistic enhancements in electrical conductivity and tensile strength [146]. However, more CNTs loading would exacerbate the aggregation and the bridging effect of GNPs is replaced by the thermal transport inhibition effect of the clusters [93,112]. On the other hand, GNPs with larger surface area and lower particle/matrix interface resistance still promote the phonon conversion mechanism [147], resulting in a more uniform heat flux distribution within the polymer (Fig. 7(b)).

Interestingly, the sequence of adding different fillers also had different effects on thermal enhancement [148]. According to the research of Xiao et al., the post-added CNTs in the ternary mixture can exfoliate and disperse the GNPs, and the $\pi - \pi$ interaction bridging between the two materials enhanced the thermal diffusion between adjacent GNPs [149]. However, in reverse order, the larger size GNPs produced a volume exclusion reaction during the assembly process, which promoted the agglomeration of CNTs and thus weakening the thermal enhancement effect (Fig. 7(c)).

In addition to the synergistic enhancement with GNPs, other thermally conductive materials such as boron nitride, expanded graphite, etc. can form new filler synergistic strengthening effect combined with CNTs. Similar to the synergistic mechanism of CNT/GNPs filler, the relatively small CNTs plays a vital bridging effect to build a multiple network structure of binary fillers [150–152]. Furthermore, The control of the addition content of large-sized fillers (e.g. expanded graphite) enables CNTs build a network around them, and cross-link with the filler network (Fig. 8(a)), improving the electrical and thermal conductivities and tensile strength [151]. When the arrangement of the filler is oriented, the thermal enhancement effect will be greatly improved. After 2D boron nitrides and 1D CNTs were arranged along the rolling direction through hot pressing and hot rolling (Fig. 8(b)), they formed a structure with overlapping orientations was formed, which formed a stronger bridging effect of CNTs and a large number of continuous filler thermal chains, thereby increasing the overall thermal conductivity by 6-fold [152].

When CNTs become large-sized fillers, other fillers can achieve secondary heat transfer in the substrate in addition to bridging function. For example, the hydrothermal reaction was used to synthesize CNT as the skeleton, MoS_2 and graphene as secondary branches for collecting the heat of the substrate and dissipated it into the CNT (Fig. 8(c)). Due to the wettability of MoS_2, the connection between the filler and the substrate was chemical bonding, which greatly reduced the ITR. Under the action of large-surface-area of MoS_2, heat transfer network of graphene and chemical bonding, the TC was increased by 23 times compared with the substrate [153].

In terms of self-healing research, the presence of CNTs restored weak hydrogen bonds between the separated surfaces in the

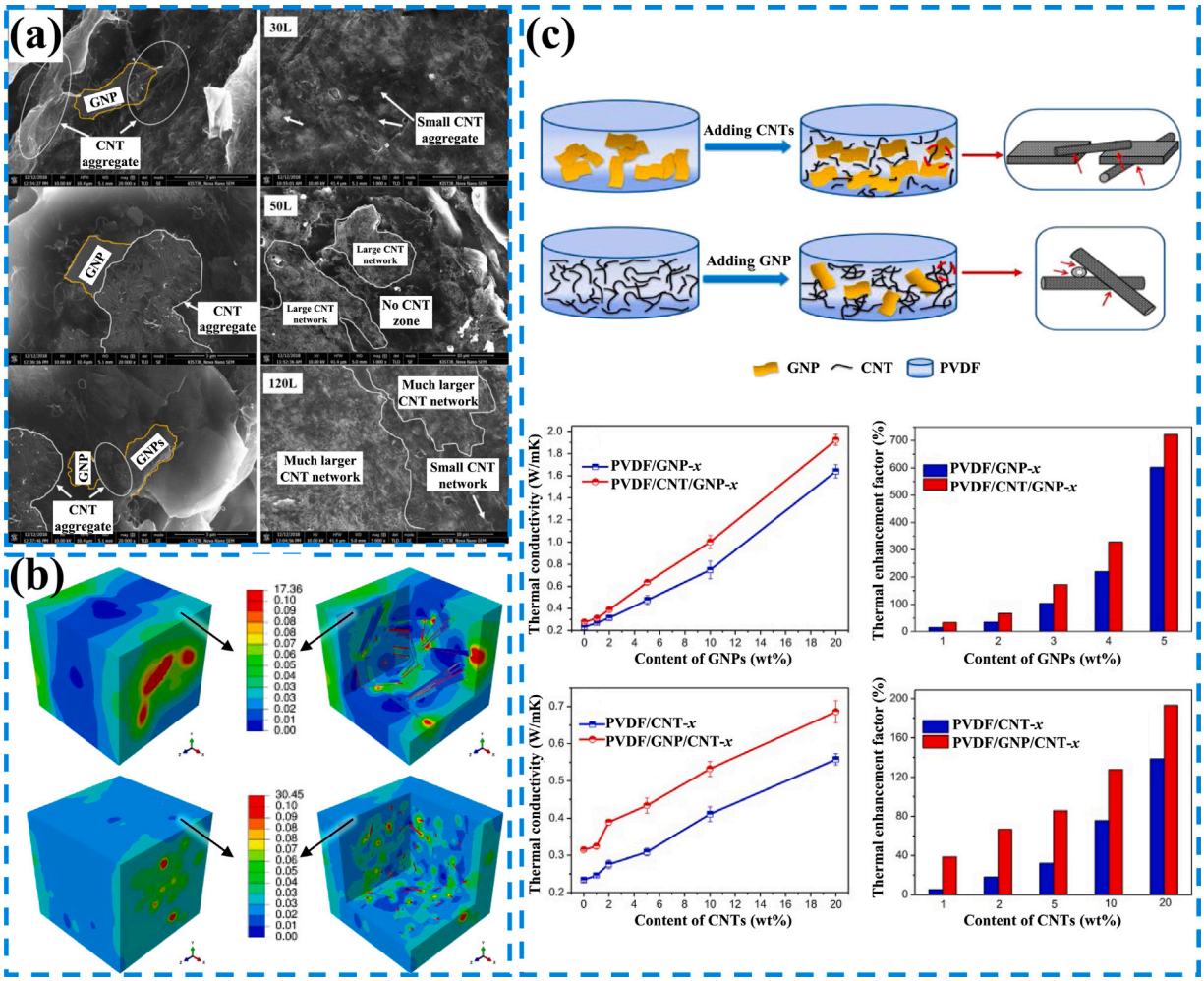

Fig. 7. Example of interfacial bonding (a) Bridging effect of GNPs (left) and aggregation regions of CNTs in composites with different lengths (right), (b) Effect of CNT/GNPs filler on heat flux uniformity based on finite element simulation (above: the hybrid configuration with 5 wt% GNPs and 0.5 wt% CNT, below: the binary configuration with 5 wt% CNTs), (c) Schematic representations showing the different dispersion states of fillers in the composites (above) and the corresponding TC measurement results and thermal enhancement effects (below).
Source: Reprinted with permission from Ref. [146] (Copyright (2019) Elsevier), Ref. [147] (Copyright (2013) Elsevier), Ref. [148] (Copyright (2016) Elsevier).

polyurethane matrix and rebuilt the bonds between the nanotube surfaces and the polyurethane, and stronger electrostatic interactions occurred at contacted interfaces. These atomic-level force changes strengthen the phonon–phonon mechanism, resulting in an enhancement of TC. The presence of CNTs slightly inhibit the mobility and diffusivity of polymer chains [154]. On the smart modulation of CNTs arrays as TIMs, the addition of polyimide materials can make arrays to withstand a pressure of 2.5 MPa. Under the action of a weak molecular cross-linked network, it withstood 30% shape deformation and restore to the original state for 24 h. In addition, the orientation structure of the array heightened the overall TC to 12.5 ± 0.18 W m^{-1} K^{-1}. The strong adhesion and high elasticity of the composite enhanced the transport of phonons across the interface and greatly reduced the thermal contact resistance (its value was $6.83 \pm 0.15 \times 10^{-6}$ K m^2 W^{-1}, which is close to the covalent bonding effect) [155].

4.3. Thermal bridges for heat sink–heat source interface

The mechanism of ITC is more specific at the end because of the complexity of contact materials, resulting in great inherent variability between contact objects, and differences in atomic-level interactions. Taking CNT arrays as an example, the adhesion interaction of the array bottom is sourced from covalent bonding to the catalyst particles, compared with the weak van der Waals force. There is a large difference in the ITC of the two interfaces from top and bottom [50,156].

According to MD simulation results, the ITR of the VACNT boots-silicon substrate decreased by 2 orders of magnitude compared with no bonding, which is benefited from chemical bonding (bonding C–Si monomolecular thin layer) [157]. Similarly, the covalent bond was used to connect the GNP surface with the CNT end (Fig. 9(a)) to construct a hybrid TIM [158]. Compared with the case without covalent bond, the ITR of CNT-graphene with this structure decreased by 3 orders of magnitude, and the overall thermal transport capacity of TIM increased by 2–3 orders of magnitude. In the experimental outcomes, it can be observed that the ITR has reached a very low limit under binding (Fig. 9(b)). The introduction of polymer [159] and metal thin layers [73] achieved bonding improvement. The research on the bonding between the array and metal can effectively reduce the hinder degree of ITR, which occurs between the metal heat sink and the array TIMs [35,160]. Therefore, it facilitates the transfer of arrays grown from the silicon substrates to the metal devices [160]. The catalyst improves the growth of the array, but has a negative feedback effect on the bonding of growing CNT roots [70].

In addition to the highly aligned arrays of surface flatness achieved by growth control (which can be seen in Table 1), post-processing methods of the interface (such as highly thermally conductive coatings or mechanical treatments) further enhance interfacial thermal transport.

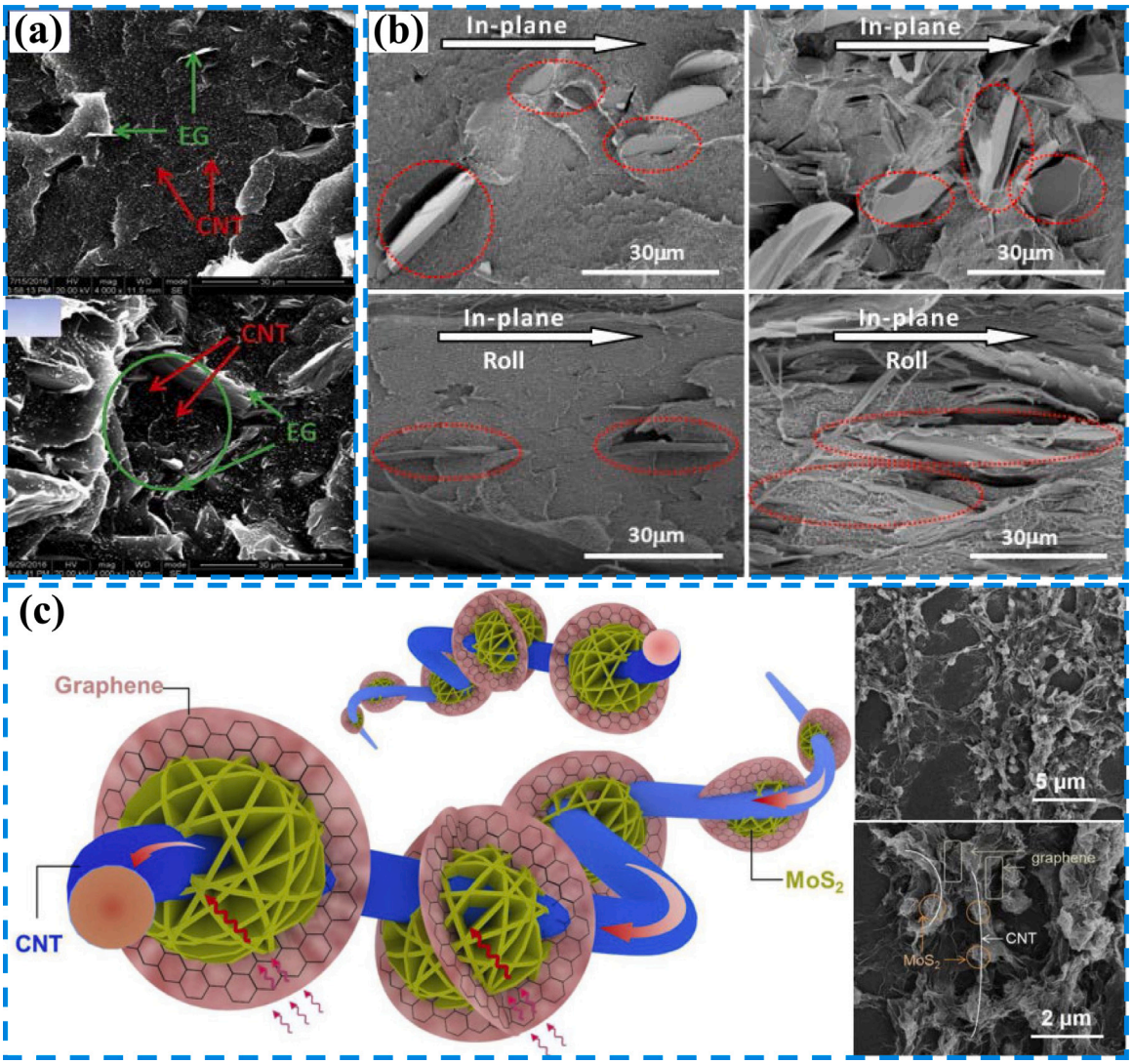

Fig. 8. Example of interfacial bonding (a) Overlapping network of expanded graphites and CNTs, (b) Boron nitrides and CNTs are oriented along the hot rolling direction, (c) Structural diagram of CNT/MoS_2/graphene nanofiller and heat transfer process in the epoxy resin matrix.
Source: Reprinted with permission from Ref. [151] (Copyright (2017) Elsevier), Ref. [152] (Copyright (2018) Elsevier), Ref. [153] (Copyright (2019) Elsevier).

Table 2 collects some results about the end ITC of pristine material, and improvements from coating or mechanical methods. According to the previous results, a good contact area can improve ITC by more than an order of magnitude. For the coating filling, two kinds of coating film including Diamond-like carbon and Titanium nitride were deposited via filtered cathodic vacuum arc technique (Fig. 9(c)). The deposition time was controlled so that the sp^2 sites in the carbon nanotube clusters form a sp^3 matrix in the coating, it turned out to be ~13 times higher than pristine [161]. Similarly, the improving of ~1.8 times, ~39 times and ~53 times were accomplished at the Al (Fig. 9(d)), carbon and reactive metal coating [163,164,166], respectively. The electron beamed process was applied to solder Bi/Sn/Ag layers and Ti/Ni/Au layers on two tips of CNTs contacted with heat sink/source [162], the different pressure (about double as the pressure increasing) and reflowing in a seven-zone reflow oven at a peak temperature of 249.85 °C (about ~1.6 times improving after reflow) were induced in these composite materials to further improve ITC.

Ti/Au coating was sputtered on to the top of the array, but only penetrating in the order of 100 nm depth into the array [70]. The array was bonded to an opposing surface at a temperature of 200 °C and a pressure of 100 kPa, the highest ITC of 10.5×10^6 W m^{-2} K^{-1} was attained. In addition to the array surface coating treatment, shear pressing on the top of array (Fig. 9(e)) was adopted to achieve compact horizontal packing and transverse physical overlapping dramatically, which increased ITC to $1.25 \pm 0.31 \times 10^6$ W m^{-2} K^{-1} [165]. Altering the sublimation temperature catalyst ferrocene greatly eliminated carbonaceous byproducts agglomerates covered the CNT tops and the Fe nanoparticles on the exterior of the CNTs are also greatly reduced, which increased ITC from $0.23 \pm 0.31 \times 10^6$ W m^{-2} K^{-1} to $0.59 \pm 0.31 \times 10^6$ W m^{-2} K^{-1} [167].

This section reviews CNT composites with material modification as the main focus. The resonant coupling between CNTs, the structural synergy between CNTs and other thermally conductive materials, and the thermal channel construction between CNTs and heat sink are achieved through the modification at the interface. All these strategies remarkably enhance the thermal transport of the composites.

5. Conclusion

This paper has reviewed the thermal transport mechanism and influencing factors of CNTs and their composites. In addition to summarizing the differences in phonon transport within the material and at the interface, it has also been observed that the size of CNTs, the interface and the arrangement between individual CNTs have different influences

Table 2
Interface treatment approaches and interfacial thermal conduction at array surface.

Research team	Interface handling		Array thickness (μm)	ITC (W m^{-2} K^{-1})
Qiu et al. [161]	Pristine		6.4	$0.31 \pm 0.02 \times 10^6$
	DLC 15 min[a]		5.6	$1.02 \pm 0.04 \times 10^6$
	DLC 30 min		7.8	$4.13 \pm 0.77 \times 10^6$
	DLC 45 min		6.4	$3.41 \pm 0.61 \times 10^6$
	DLC 60 min		7.1	$1.03 \pm 0.06 \times 10^6$
	TiN 20 min		8.5	$2.54 \pm 0.22 \times 10^6$
	TiN 30 min		9.0	$1.01 \pm 0.49 \times 10^6$
Peacock et al. [162]	Bi/Sn/Ag	Initial, 0.14 MPa	25	$1.33 \pm 0.13 \times 10^4$
		Initial, 0.34 MPa		$1.37 \pm 0.13 \times 10^4$
	Ti/Ni/Au[b]	After reflow, 0.14 MPa		$2.18 \pm 0.21 \times 10^4$
		After reflow, 0.34 MPa		$2.33 \pm 0.23 \times 10^4$
Wu et al. [163]	Pristine		\	0.66×10^6
	Al-coating[c]		\	1.2×10^6
Ping et al. [164]	Pristine		20	0.02×10^6
	C-coating		20	0.31×10^6
	C-coating		40	0.48×10^6
	C-coating		80	0.77×10^6
Nylander et al. [70]	Single-bonded Si-CNT-Si		80	$3.74 \pm 1.50 \times 10^6$
	Double-bonded Si-CNT-Si		80	$3.08 \pm 0.84 \times 10^6$
	Single-bonded Si-CNT-Cu		80	$3.49 \pm 0.59 \times 10^6$
	Single-bonded Si-CNT-Cu		200	1.92×10^6
	Single-bonded Si-CNT-Cu		50	8.13×10^6
	Single-bonded Si-CNT-Cu		10	10.53×10^6
	Double-bonded Si-CNT-Cu		80	$2.01 \pm 0.40 \times 10^6$
Qiu et al. [165]	Shear pressing		45	$1.25 \pm 0.31 \times 10^6$
Barako et al. [166]	Pristine		\	$0.07 - 0.20 \times 10^4$
	Growth interface		\	$0.54 - 0.77 \times 10^4$
	Indium bonding		\	$2.13 - 3.33 \times 10^4$
	Reactive metal bonding		\	$2.44 - 3.70 \times 10^4$
Qiu et al. [167]	Pristine		\	0.23×10^6
	Eliminating C-BPs agglomerates[d] &Fe		\	0.59×10^6

[a]15 min deposition time via Diamond-like carbon (DLC) or TiN, the following related content is the same.
[b]Bi/Sn/Ag solder (127 μm)-Ti/Ni/Au (0.3 μm)-CNTs (25 μm)-Ti/Ni/Au (0.3 μm)–Bi/Sn/Ag solder (127 μm).
[c]Uniform aluminum layer is introduced to the surface of array.
[d]Carbonaceous byproducts (C-BPs).

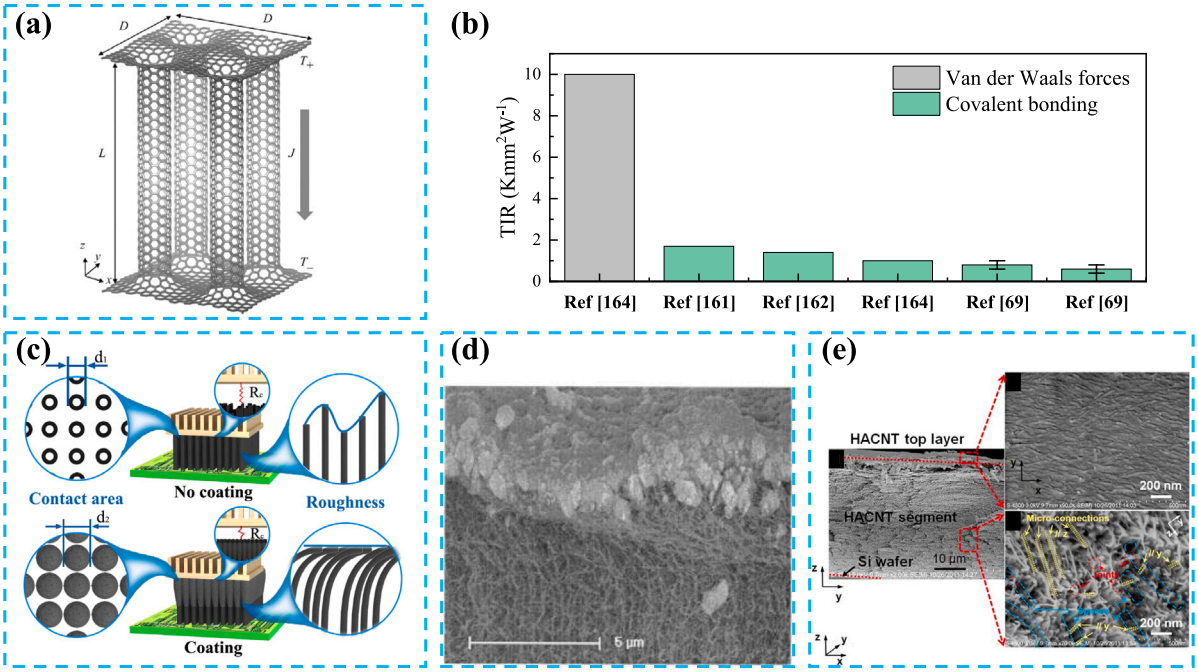

Fig. 9. Thermal enhancement strategies at the interface between heat sink and TIM (a) Schematic of the setup for the MD simulations. Langevin thermostat with temperature T_+ and T_- is applied to the top and bottom GNPs, respectively, resulting in the heat flow J in the z-direction, (b) Comparison of interfacial thermal resistance under van der Waals force and covalent bonding, (c) Diamond-like carbon and Titanium nitride and (d) 1-μm-thick aluminum layer coating filling on top of the array for interfacial thermal enhancement, (e) Horizontally aligned CNTs sheared pressing on the array top.
Source: Reprinted with permission from Ref. [158] (Copyright (2015) Wiley Online Library), Ref. [161] (Copyright (2019) Elsevier), Ref. [163] (Copyright (2005) American Institute of Physics), Ref. [165] (Copyright (2016) Nature).

on the overall TC. It is concluded that: (1) Most CNT materials have a quadratic dependence of length, but the effect of CNT diameter on the overall thermal transport should also account the phonon scattering effect between nanotubes; (2) In the composites, the interface between the individual CNTs is the biggest obstacle to the overall thermal transport, and due to the limitation of weak van der Waals force, the ITC cannot simply be enhanced by mechanical methods; (3) the spatial distribution of inter-CNT junctions in composites interferes with the propagation distance of interface phonons. (4) High density and order of CNTs composites have good thermal transport properties, but the aggregation phenomenon caused by a random distribution of CNTs inhibits the overall thermal transport effect.

Based on the above thermal transport mechanism, this review also investigates the related thermal enhancement strategies. The growth control and interface optimization of CNTs are the research hotspots of composite materials in recent years, which mainly include: (1) Control the uniformity and orientation of CNTs growth to improve the interfacial contact and achieve directional thermal transport, which increases the anisotropy ratio of composites; (2) The interface modification increases the strength of interfacial atomic forces, and the addition of additional interfacial thermal channels to suppress the interference of phonon scattering; (3) Structural synergy strategies make CNTs and other highly thermally conductive materials in composites to build efficient thermal transport networks. In addition, the paper also presents the functional synergistic effects of self-healing and mechanical enhancement of recently developed smart TIM materials in practical thermal management applications.

Declaration of competing interest

The authors declare that they have no known competing financial interests or personal relationships that could have appeared to influence the work reported in this paper.

Data availability

Data will be made available on request.

Acknowledgments

This study was supported by National Natural Science Foundation of China (52222602), Beijing Natural Science Foundation (3202020), Interdisciplinary Research Project for Young Teachers of USTB (Fundamental Research Funds for the Central Universities, FRF-IDRY-GD21-004).

References

[1] M. Ebadian, C. Lin, A review of high-heat-flux heat removal technologies, J. Heat Transfer 133 (11) (2011) http://dx.doi.org/10.1115/1.4004340.

[2] Q. Yang, J. Zhao, Y. Huang, X. Zhu, W. Fu, C. Li, J. Miao, A diamond made microchannel heat sink for high-density heat flux dissipation, Appl. Therm. Eng. 158 (2019) 113804, http://dx.doi.org/10.1016/j.applthermaleng.2019.113804.

[3] S. Berber, Y. Kwon, D. Tománek, Unusually high thermal conductivity of carbon nanotubes, Phys. Rev. Lett. 84 (20) (2000) 4613–4616, http://dx.doi.org/10.1103/PhysRevLett.84.4613.

[4] C. Yu, L. Shi, Z. Yao, D. Li, A. Majumdar, Thermal conductance and thermopower of an individual single-wall carbon nanotube, Nano Lett. 5 (2005) 1842–1846, http://dx.doi.org/10.1021/nl051044e.

[5] P. Kim, L. Shi, A. Majumdar, P.L. McEuen, Thermal transport measurements of individual multiwalled nanotubes, Phys. Rev. Lett. 87 (2001) 215502, http://dx.doi.org/10.1103/PhysRevLett.87.215502.

[6] J. Hone, M. Whitney, A. Zettl, Thermal conductivity of single-walled carbon nanotubes, Synth. Met. 103 (1) (1999) 2498–2499, http://dx.doi.org/10.1016/S0379-6779(98)01070-4.

[7] M. Kusunoki, M. Rokkaku, T. Suzuki, Epitaxial carbon nanotube film self-organized by sublimation decomposition of silicon carbide, Appl. Phys. Lett. 71 (18) (1997) 2620–2622, http://dx.doi.org/10.1063/1.120158.

[8] W. Zhou, J. Vavro, C. Guthy, K.I. Winey, J.E. Fischer, L.M. Ericson, S. Ramesh, R. Saini, V.A. Davis, C. Kittrell, M. Pasquali, R.H. Hauge, R.E. Smalley, Single wall carbon nanotube fibers extruded from super-acid suspensions: Preferred orientation, electrical, and thermal transport, J. Appl. Phys. 95 (2) (2004) 649–655, http://dx.doi.org/10.1063/1.1627457.

[9] R. Wang, S. Zheng, Y. Zheng, Introduction to polymer matrix composites, in: R. Wang, S. Zheng, Y. Zheng (Eds.), Polymer Matrix Composites and Technology, in: Woodhead Publishing Series in Composites Science and Engineering, Woodhead Publishing, 2011, pp. 1–548, http://dx.doi.org/10.1533/9780857092229.1.

[10] M.A. Usmani, I. Khan, A. Haque, A.H. Bhat, D. Mondal, U. Gazal, 4 - biomass-based composites from different sources: Properties, characterization, and transforming biomass with ionic liquids, in: M. Jawaid, P. Md Tahir, N. Saba (Eds.), Lignocellulosic Fibre and Biomass-Based Composite Materials, in: Woodhead Publishing Series in Composites Science and Engineering, Woodhead Publishing, 2017, pp. 45–76, http://dx.doi.org/10.1016/B978-0-08-100959-8.00004-4.

[11] L. Qiu, P. Guo, X. Yang, Y. Ouyang, Y. Feng, X. Zhang, J. Zhao, X. Zhang, Q. Li, Electro curing of oriented bismaleimide between aligned carbon nanotubes for high mechanical and thermal performances, Carbon 145 (2019) 650–657, http://dx.doi.org/10.1016/j.carbon.2019.01.074.

[12] N. Behabtu, C.C. Young, D.E. Tsentalovich, O. Kleinerman, X. Wang, A.W.K. Ma, E.A. Bengio, R.F. ter Waarbeek, J.J. de Jong, R.E. Hoogerwerf, S.B. Fairchild, J.B. Ferguson, B. Maruyama, J. Kono, Y. Talmon, Y. Cohen, M.J. Otto, M. Pasquali, Strong, light, multifunctional fibers of carbon nanotubes with ultrahigh conductivity, Science 339 (6116) (2013) 182–186, http://dx.doi.org/10.1126/science.1228061.

[13] D. Salmon, Thermal conductivity of insulations using guarded hot plates, including recent developments and sources of reference materials, Meas. Sci. Technol. 12 (12) (2001) R89–R98, http://dx.doi.org/10.1088/0957-0233/12/12/201.

[14] W. Guo, G. Li, Y. Zheng, C. Dong, Measurement of the thermal conductivity of SiO_2 nanofluids with an optimized transient hot wire method, Thermochim. Acta 661 (2018) 84–97, http://dx.doi.org/10.1016/j.tca.2018.01.008.

[15] K. Antoniadis, G. Tertsinidou, M. Assael, W. Wakeham, Transient hot-wire measurements of the apparent thermal conductivity of nanofluids are seldom satisfied, Int. J. Thermophys. 37 (2016) 78, http://dx.doi.org/10.1007/s10765-016-2083-8.

[16] J. Lee, H. Lee, Y.-J. Baik, J. Koo, Quantitative analyses of factors affecting thermal conductivity of nanofluids using an improved transient hot-wire method apparatus, Int. J. Heat Mass Transfer 89 (2015) 116–123, http://dx.doi.org/10.1016/j.ijheatmasstransfer.2015.05.064.

[17] Z. Aparna, M.M. Michael, S.K. Pabi, S. Ghosh, Diversity in thermal conductivity of aqueous Al_2O_3- and Ag-nanofluids measured by transient hot-wire and laser flash methods, Exp. Therm. Fluid Sci. 94 (2018) 231–245, http://dx.doi.org/10.1016/j.expthermflusci.2018.02.005.

[18] E.M. Hemmat, S. Saedodin, O. Mahian, S. Wongwises, Thermal conductivity of Al_2O_3/water nanofluids, J. Therm. Anal. Calorim. 117 (2014) 675–681, http://dx.doi.org/10.1016/10.1007/s10973-014-3771-x.

[19] X. Zhang, S. Fujiwara, M. Fujii, Measurements of thermal conductivity and electrical conductivity of a single carbon fiber, Int. J. Thermophys. 21 (2000) 965–980, http://dx.doi.org/10.1023/A:1006674510648.

[20] J. Wang, M. Gu, X. Zhang, Y. Song, Thermal conductivity measurement of an individual fibre using a T type probe method, J. Phys. D Appl. Phys. 42 (10) (2009) 105502, http://dx.doi.org/10.1088/0022-3727/42/10/105502.

[21] M. Fujii, X. Zhang, H. Xie, H. Ago, K. Takahashi, T. Ikuta, H. Abe, T. Shimizu, Measuring the thermal conductivity of a single carbon nanotube, Phys. Rev. Lett. 95 (2005) 065502, http://dx.doi.org/10.1103/PhysRevLett.95.065502.

[22] H. Wang, S. Hu, K. Takahashi, X. Zhang, H. Takamatsu, J. Chen, Experimental study of thermal rectification in suspended monolayer graphene, Nature Commun. 8 (2017) 15843, http://dx.doi.org/10.1038/ncomms15843.

[23] D.G. Cahill, R.O. Pohl, Thermal conductivity of amorphous solids above the plateau, Phys. Rev. B 35 (1987) 4067–4073, http://dx.doi.org/10.1103/PhysRevB.35.4067.

[24] D.G. Cahill, Thermal conductivity measurement from 30 to 750 K: the 3ω method, Rev. Sci. Instrum. 61 (2) (1990) 802–808, http://dx.doi.org/10.1063/1.1141498.

[25] S. Ahmed, R. Liske, T. Wunderer, M. Leonhardt, R. Ziervogel, C. Fansler, T. Grotjohn, J. Asmussen, T. Schuelke, Extending the 3ω method to the MHz range for thermal conductivity measurements of diamond thin films, Diam. Relat. Mater. 15 (2) (2006) 389–393, http://dx.doi.org/10.1016/j.diamond.2005.08.041.

[26] B.W. Olson, S. Graham, K. Chen, A practical extension of the 3ω method to multilayer structures, Rev. Sci. Instrum. 76 (5) (2005) 053901, http://dx.doi.org/10.1063/1.1896619.

[27] L. Qiu, Y. Ouyang, Y. Feng, X. Zhang, Note: Thermal conductivity measurement of individual porous polyimide fibers using a modified wire-shape 3ω method, Rev. Sci. Instrum. 89 (9) (2018) 096112, http://dx.doi.org/10.1063/1.5052692.

[28] W.J. Parker, R.J. Jenkins, C.P. Butler, G.L. Abbott, Flash method of determining thermal diffusivity, heat capacity, and thermal conductivity, J. Appl. Phys. 32 (9) (1961) 1679–1684, http://dx.doi.org/10.1063/1.1728417.

[29] J. Blumm, A. Lindemann, S. Min, Thermal characterization of liquids and pastes using the flash technique, Thermochim. Acta 455 (1) (2007) 26–29, http://dx.doi.org/10.1016/j.tca.2006.11.023.

[30] W. Lin, J. Shang, W. Gu, C. Wong, Parametric study of intrinsic thermal transport in vertically aligned multi-walled carbon nanotubes using a laser flash technique, Carbon 50 (4) (2012) 1591–1603, http://dx.doi.org/10.1016/j.carbon.2011.11.038.

[31] H. Xie, A. Cai, X. Wang, Thermal diffusivity and conductivity of multiwalled carbon nanotube arrays, Phys. Lett. A 369 (1) (2007) 120–123, http://dx.doi.org/10.1016/j.physleta.2007.02.079.

[32] M. Akoshima, K. Hata, D.N. Futaba, K. Mizuno, T. Baba, M. Yumura, Thermal diffusivity of single-walled carbon nanotube forest measured by laser flash method, Japan. J. Appl. Phys. 48 (5) (2009) 05EC07, http://dx.doi.org/10.1143/jjap.48.05ec07.

[33] Y. Jannot, A. Degiovanni, Steady-state methods, in: Thermal Properties Measurement of Materials, John Wiley & Sons, Ltd, 2018, pp. 83–116, http://dx.doi.org/10.1002/9781119475057.ch3, Chapter 3.

[34] R. Prasher, T. Tong, A. Majumdar, An acoustic and dimensional mismatch model for thermal boundary conductance between a vertical mesoscopic nanowire/nanotube and a bulk substrate, J. Appl. Phys. 102 (10) (2007) 104312, http://dx.doi.org/10.1063/1.2816260.

[35] S. Kaur, N. Raravikar, B.A. Helms, R. Prasher, D.F. Ogletree, Enhanced thermal transport at covalently functionalized carbon nanotube array interfaces, Nature Commun. 5 (1) (2014) 3082, http://dx.doi.org/10.1038/ncomms4082.

[36] G. Mahan, Thermoelectric effect, in: F. Bassani, G.L. Liedl, P. Wyder (Eds.), Encyclopedia of Condensed Matter Physics, Elsevier, Oxford, 2005, pp. 180–187, http://dx.doi.org/10.1016/B0-12-369401-9/00726-9.

[37] H. Heinz, R.A. Vaia, B.L. Farmer, R.R. Naik, Accurate simulation of surfaces and interfaces of face-centered cubic metals using 12–6 and 9–6 Lennard-Jones potentials, J. Phys. Chem. C 112 (44) (2008) 17281–17290, http://dx.doi.org/10.1021/jp801931d.

[38] K. Kanhaiya, S. Kim, W. Im, H. Heinz, Accurate simulation of surfaces and interfaces of ten FCC metals and steel using Lennard – Jones potentials, NPJ Comput. Mater. 7 (1) (2021) 17, http://dx.doi.org/10.1038/s41524-020-00478-1.

[39] P. Mausbach, R. Fingerhut, J. Vrabec, Structure and dynamics of the Lennard-Jones fcc-solid focusing on melting precursors, J. Chem. Phys. 153 (10) (2020) 104506, http://dx.doi.org/10.1063/5.0015371.

[40] T.A. Halgren, The representation of vanderWaals(vdW) interactions in molecular mechanics force fields: potential form, combination rules, and vdW parameters, J. Am. Chem. Soc. 114 (20) (1992) 7827–7843, http://dx.doi.org/10.1021/ja00046a032.

[41] K. Laasonen, S. Wonczak, R. Strey, A. Laaksonen, Molecular dynamics simulations of gas–liquid nucleation of Lennard-Jones fluid, J. Chem. Phys. 113 (21) (2000) 9741–9747, http://dx.doi.org/10.1063/1.1322082.

[42] A. Liu, S.J. Stuart, Empirical bond-order potential for hydrocarbons: Adaptive treatment of vanderWaals interactions, J. Comput. Chem. 29 (4) (2008) 601–611, http://dx.doi.org/10.1002/jcc.20817.

[43] S.P. Fu, Z. Peng, H. Yuan, R. Kfoury, Y.N. Young, Lennard-Jones type pair-potential method for coarse-grained lipid bilayer membrane simulations in LAMMPS, Comput. Phys. Comm. 210 (2017) 193–203, http://dx.doi.org/10.1016/j.cpc.2016.09.018.

[44] M. Kazan, P. Masri, The contribution of surfaces and interfaces to the crystal thermal conductivity, Surf. Sci. Rep. 69 (1) (2014) 1–37, http://dx.doi.org/10.1016/j.surfrep.2013.11.001.

[45] V. Varshney, S.S. Patnaik, A.K. Roy, B.L. Farmer, Modeling of thermal conductance at transverse CNT – –CNT interfaces, J. Phys. Chem. C 114 (39) (2010) 16223–16228, http://dx.doi.org/10.1021/jp104139x.

[46] A. Tamura, T. Ichinokawa, Frequency spectrum of a small particle, J. Phys. C Solids Stat. Phys. 16 (24) (1983) 4779–4788, http://dx.doi.org/10.1088/0022-3719/16/24/011.

[47] X. Wu, T. Luo, Effect of electron-phonon coupling on thermal transport across metal-nonmetal interface — A second look, Europhys. Lett. 110 (6) (2015) 67004, http://dx.doi.org/10.1209/0295-5075/110/67004.

[48] W. Chen, J. Yang, Z. Wei, C. Liu, K. Bi, Y. Chen, Axial tensile strain effects on the contact thermal conductance between cross contacted single-walled carbon nanotubes, J. Appl. Phys. 121 (5) (2017) 054310, http://dx.doi.org/10.1063/1.4975466.

[49] W.A. Little, The transport of heat between dissimilar solids at low temperatures, Can. J. Phys. 37 (3) (1959) 334–349, http://dx.doi.org/10.1139/p59-037.

[50] R. Prasher, Acoustic mismatch model for thermal contact resistance of van der Waals contacts, Appl. Phys. Lett. 94 (4) (2009) 041905, http://dx.doi.org/10.1063/1.3075065.

[51] R.J. Stoner, H.J. Maris, Kapitza conductance and heat flow between solids at temperatures from 50 to 300 K, Phys. Rev. B 48 (1993) 16373–16387, http://dx.doi.org/10.1103/PhysRevB.48.16373.

[52] R.J. Stevens, A.N. Smith, P.M. Norris, Measurement of thermal boundary conductance of a series of metal-dielectric interfaces by the transient thermoreflectance technique, J. Heat Transfer 127 (3) (2005) 315–322, http://dx.doi.org/10.1115/1.1857944.

[53] W. Hsieh, A.S. Lyons, E. Pop, P. Keblinski, D.G. Cahill, Pressure tuning of the thermal conductance of weak interfaces, Phys. Rev. B 84 (2011) 184107, http://dx.doi.org/10.1103/PhysRevB.84.184107.

[54] B. Liu, N. Vu-Bac, X. Zhuang, X. Fu, T. Rabczuk, Stochastic integrated machine learning based multiscale approach for the prediction of the thermal conductivity in carbon nanotube reinforced polymeric composites, Compos. Sci. Technol. 224 (2022) 109425, http://dx.doi.org/10.1016/j.compscitech.2022.109425.

[55] B. Liu, N. Vu-Bac, X. Zhuang, X. Fu, T. Rabczuk, Stochastic full-range multiscale modeling of thermal conductivity of polymeric carbon nanotubes composites: A machine learning approach, Compos. Struct. 289 (2022) 115393, http://dx.doi.org/10.1016/j.compstruct.2022.115393.

[56] L.E. Vivanco-Benavides, C.L. Martínez-González, C. Mercado-Zúñiga, C. Torres-Torres, Machine learning and materials informatics approaches in the analysis of physical properties of carbon nanotubes: A review, Comput. Mater. Sci. 201 (2022) 110939, http://dx.doi.org/10.1016/j.commatsci.2021.110939.

[57] A. Karimipour, S.A. Bagherzadeh, A. Taghipour, A. Abdollahi, M.R. Safaei, A novel nonlinear regression model of SVR as a substitute for ANN to predict conductivity of MWCNT-cuo/water hybrid nanofluid based on empirical data, Physica A 521 (2019) 89–97, http://dx.doi.org/10.1016/j.physa.2019.01.055.

[58] H. Zou, C. Chen, M. Zha, K. Zhou, R. Xiao, Y. Feng, L. Qiu, X. Zhang, Z. Wang, A neural regression model for predicting thermal conductivity of CNT nanofluids with multiple base fluids, J Therm. Sci. 30 (6) (2021) 1908–1916, http://dx.doi.org/10.1007/s11630-021-1497-1.

[59] S. Rostami, R. Kalbasi, M. Talebkeikhah, A.S. Goldanlou, Improving the thermal conductivity of ethylene glycol by addition of hybrid nano-materials containing multi-walled carbon nanotubes and titanium dioxide: applicable for cooling and heating, J Therm. Anal. Calorim. 143 (2) (2021) 1701–1712, http://dx.doi.org/10.1007/s10973-020-09921-3.

[60] A. Baghban, M. Kahani, M.A. Nazari, M.H. Ahmadi, W.-M. Yan, Sensitivity analysis and application of machine learning methods to predict the heat transfer performance of CNT/water nanofluid flows through coils, Int. J. Heat Mass Transfer 128 (2019) 825–835, http://dx.doi.org/10.1016/j.ijheatmasstransfer.2018.09.041.

[61] M.H. Pebdani, R.E. Miller, Molecular dynamics simulation of pull-out halloysite nanotube from polyurethane matrix, Adv. Mech. Eng. 13 (9) (2021) 16878140211044663, http://dx.doi.org/10.1177/16878140211044663.

[62] A. Rahman, P. Deshpande, M.S. Radue, G.M. Odegard, S. Gowtham, S. Ghosh, A.D. Spear, A machine learning framework for predicting the shear strength of carbon nanotube-polymer interfaces based on molecular dynamics simulation data, Compos. Sci. Technol. 207 (2021) 108627, http://dx.doi.org/10.1016/j.compscitech.2020.108627.

[63] V. Varshney, J. Lee, D. Li, J.S. Brown, B.L. Farmer, A.A. Voevodin, A.K. Roy, Understanding thermal conductance across multi-wall carbon nanotube contacts: Role of nanotube curvature, Carbon 114 (2017) 15–22, http://dx.doi.org/10.1016/j.carbon.2016.11.056.

[64] J.F. Niven, M.B. Johnson, S.M. Juckes, M.A. White, N.T. Alvarez, V. Shanov, Influence of annealing on thermal and electrical properties of carbon nanotube yarns, Carbon 99 (2016) 485–490, http://dx.doi.org/10.1016/j.carbon.2015.12.014.

[65] Z. Zhang, Y. Ouyang, Y. Cheng, J. Chen, N. Li, G. Zhang, Size-dependent phononic thermal transport in low-dimensional nanomaterials, Phys. Rep. 860 (2020) 1–26, http://dx.doi.org/10.1016/j.physrep.2020.03.001.

[66] G. Zhang, B. Li, Thermal conductivity of nanotubes revisited: Effects of chirality, isotope impurity, tube length, and temperature, J. Chem. Phys. 123 (11) (2005) 114714, http://dx.doi.org/10.1063/1.2036967.

[67] C.W. Chang, D. Okawa, H. Garcia, A. Majumdar, A. Zettl, Breakdown of Fourier's law in nanotube thermal conductors, Phys. Rev. Lett. 101 (2008) 075903, http://dx.doi.org/10.1103/PhysRevLett.101.075903.

[68] L. Qiu, X. Wang, D. Tang, X. Zheng, P.M. Norris, D. Wen, J. Zhao, X. Zhang, Q. Li, Functionalization and densification of inter-bundle interfaces for improvement in electrical and thermal transport of carbon nanotube fibers, Carbon 105 (2016) 248–259, http://dx.doi.org/10.1016/j.carbon.2016.04.043.

[69] L. Qiu, H. Zou, N. Zhu, Y. Feng, X. Zhang, X. Zhang, Iodine nanoparticle-enhancing electrical and thermal transport for carbon nanotube fibers, Appl. Therm. Eng. 141 (2018) 913–920, http://dx.doi.org/10.1016/j.applthermaleng.2018.06.049.

[70] A. Nylander, J. Hansson, T. Nilsson, L. Ye, Y. Fu, J. Liu, Degradation of carbon nanotube array thermal interface materials through thermal aging: Effects of bonding, array height, and catalyst oxidation, ACS Appl. Mater. Interfaces 13 (26) (2021) 30992–31000, http://dx.doi.org/10.1021/acsami.1c05685.

[71] B.A. Cola, P.B. Amama, X. Xu, T.S. Fisher, Effects of growth temperature on carbon nanotube array thermal interfaces, J. Heat Transfer 130 (11) (2008) http://dx.doi.org/10.1115/1.2969758.

[72] J. Xu, T.S. Fisher, Enhancement of thermal interface materials with carbon nanotube arrays, Int. J. Heat Mass Transfer 49 (9) (2006) 1658–1666, http://dx.doi.org/10.1016/j.ijheatmasstransfer.2005.09.039.

[73] T. Tong, Y. Zhao, L. Delzeit, A. Kashani, M. Meyyappan, A. Majumdar, Dense vertically aligned multiwalled carbon nanotube arrays as thermal interface materials, IEEE Trans. Compon. Pack. Manuf. Technol. 30 (1) (2007) 92–100, http://dx.doi.org/10.1109/TCAPT.2007.892079.

[74] X. Huang, J. Wang, G. Eres, X. Wang, Thermophysical properties of multi-wall carbon nanotube bundles at elevated temperatures up to 830 K, Carbon 49 (5) (2011) 1680–1691, http://dx.doi.org/10.1016/j.carbon.2010.12.053.
[75] Y. Xie, T. Wang, B. Zhu, C. Yan, P. Zhang, X. Wang, G. Eres, 19-Fold thermal conductivity increase of carbon nanotube bundles toward high-end thermal design applications, Carbon 139 (2018) 445–458, http://dx.doi.org/10.1016/j.carbon.2018.07.009.
[76] N. Mingo, L. Yang, Phonon transport in nanowires coated with an amorphous material: An atomistic Green's function approach, Phys. Rev. B 68 (2003) 245406, http://dx.doi.org/10.1103/PhysRevB.68.245406.
[77] W. Zhang, T.S. Fisher, N. Mingo, Simulation of interfacial phonon transport in Si–Ge heterostructures using an atomistic Green's function method, J. Heat Transfer 129 (4) (2006) 483–491, http://dx.doi.org/10.1115/1.2709656.
[78] X. Yang, D. Chen, Z. Han, X. Ma, A.C. To, Effects of welding on thermal conductivity of randomly oriented carbon nanotube networks, Int. J. Heat Mass Transfer 70 (2014) 803–810, http://dx.doi.org/10.1016/j.ijheatmasstransfer.2013.11.071.
[79] H. Wang, A.S. Tazebay, G. Yang, H.T. Lin, W. Choi, C. Yu, Highly deformable thermal interface materials enabled by covalently-bonded carbon nanotubes, Carbon 106 (2016) 152–157, http://dx.doi.org/10.1016/j.carbon.2016.05.017.
[80] R.N. Salaway, L.V. Zhigilei, Thermal conductance of carbon nanotube contacts: Molecular dynamics simulations and general description of the contact conductance, Phys. Rev. B 94 (2016) 014308, http://dx.doi.org/10.1103/PhysRevB.94.014308.
[81] H. Zhong, J.R. Lukes, Interfacial thermal resistance between carbon nanotubes: Molecular dynamics simulations and analytical thermal modeling, Phys. Rev. B 74 (2006) 125403, http://dx.doi.org/10.1103/PhysRevB.74.125403.
[82] Z. Xu, M.J. Buehler, Nanoengineering heat transfer performance at carbon nanotube interfaces, ACS Nano 3 (9) (2009) 2767–2775, http://dx.doi.org/10.1021/nn9006237.
[83] A.N. Volkov, R.N. Salaway, L.V. Zhigilei, Atomistic simulations, mesoscopic modeling, and theoretical analysis of thermal conductivity of bundles composed of carbon nanotubes, J. Appl. Phys. 114 (10) (2013) 104301, http://dx.doi.org/10.1063/1.4819911.
[84] D. Liao, W. Chen, J. Zhang, Y. Yue, Tuning thermal conductance of CNT interface junction via stretching and atomic bonding, J. Phys. D Appl. Phys. 50 (47) (2017) 475302, http://dx.doi.org/10.1088/1361-6463/aa8ff8.
[85] W.J. Evans, M. Shen, P. Keblinski, Inter-tube thermal conductance in carbon nanotubes arrays and bundles: Effects of contact area and pressure, Appl. Phys. Lett. 100 (26) (2012) 261908, http://dx.doi.org/10.1063/1.4732100.
[86] L. Hu, A.J.H. McGaughey, Thermal conductance of the junction between single-walled carbon nanotubes, Appl. Phys. Lett. 105 (19) (2014) 193104, http://dx.doi.org/10.1063/1.4902074.
[87] W. Chen, J. Zhang, Y. Yue, Molecular dynamics study on thermal transport at carbon nanotube interface junctions: Effects of mechanical force and chemical functionalization, Int. J. Heat Mass Transfer 103 (2016) 1058–1064, http://dx.doi.org/10.1016/j.ijheatmasstransfer.2016.08.016.
[88] G. Hu, B. Cao, Thermal resistance between crossed carbon nanotubes: Molecular dynamics simulations and analytical modeling, J. Appl. Phys. 114 (22) (2013) 224308, http://dx.doi.org/10.1063/1.4842896.
[89] J. Yang, S. Waltermire, Y. Chen, A.A. Zinn, T.T. Xu, D. Li, Contact thermal resistance between individual multiwall carbon nanotubes, Appl. Phys. Lett. 96 (2) (2010) 023109, http://dx.doi.org/10.1063/1.3292203.
[90] R. Prasher, Thermal boundary resistance and thermal conductivity of multi-walled carbon nanotubes, Phys. Rev. B 77 (2008) 075424, http://dx.doi.org/10.1103/PhysRevB.77.075424.
[91] Z. Wei, Y. Chen, C. Dames, Negative correlation between in-plane bonding strength and cross-plane thermal conductivity in a model layered material, Appl. Phys. Lett. 102 (1) (2013) 011901, http://dx.doi.org/10.1063/1.4773372.
[92] Q. Rong, C. Shao, H. Bao, Molecular dynamics study of the interfacial thermal conductance of multi-walled carbon nanotubes and van der waals force induced deformation, J. Appl. Phys. 121 (5) (2017) 054302, http://dx.doi.org/10.1063/1.4975032.
[93] Q. Kong, L. Bodelot, B. Lebental, Y.D. Lim, L.L. Shiau, B. Gusarov, C.W. Tan, K. Liang, C. Lu, C.S. Tan, P. Coquet, B.K. Tay, Novel three-dimensional carbon nanotube networks as high performance thermal interface materials, Carbon 132 (2018) 359–369, http://dx.doi.org/10.1016/j.carbon.2018.02.052.
[94] W. Hong, N. Tai, Investigations on the thermal conductivity of composites reinforced with carbon nanotubes, Diam. Relat. Mater. 17 (7) (2008) 1577–1581, http://dx.doi.org/10.1016/j.diamond.2008.03.037.
[95] G. Zhang, C. Liu, S. Fan, Directly measuring of thermal pulse transfer in one-dimensional highly aligned carbon nanotubes, Sci. Rep. 3 (1) (2013) 2549, http://dx.doi.org/10.1038/srep02549.
[96] S. Shaikh, L. Li, K. Lafdi, J. Huie, Thermal conductivity of an aligned carbon nanotube array, Carbon 45 (13) (2007) 2608–2613, http://dx.doi.org/10.1016/j.carbon.2007.08.011.
[97] I. Ivanov, A. Puretzky, G. Eres, H. Wang, Z. Pan, H. Cui, R. Jin, J. Howe, D.B. Geohegan, Fast and highly anisotropic thermal transport through vertically aligned carbon nanotube arrays, Appl. Phys. Lett. 89 (22) (2006) 223110, http://dx.doi.org/10.1063/1.2397008.
[98] Z.L. Gao, K. Zhang, M.M.F. Yuen, Fabrication of carbon nanotube thermal interface material on aluminum alloy substrates with low pressure CVD, Nanotechnology 22 (26) (2011) 265611, http://dx.doi.org/10.1088/0957-4484/22/26/265611.
[99] L. Ping, P. Hou, H. Wang, M. Chen, Y. Zhao, H. Cong, C. Liu, H. Cheng, Clean, fast and scalable transfer of ultrathin/patterned vertically-aligned carbon nanotube arrays, Carbon 133 (2018) 275–282, http://dx.doi.org/10.1016/j.carbon.2018.03.032.
[100] M.B. Jakubinek, M.B. Johnson, M.A. White, C. Jayasinghe, G. Li, W. Cho, M.J. Schulz, V. Shanov, Thermal and electrical conductivity of array-spun multi-walled carbon nanotube yarns, Carbon 50 (1) (2012) 244–248, http://dx.doi.org/10.1016/j.carbon.2011.08.041.
[101] I. Jang, S.B. Sinnott, D. Danailov, P. Keblinski, Molecular dynamics simulation study of carbon nanotube welding under electron beam irradiation, Nano Lett. 4 (1) (2004) 109–114, http://dx.doi.org/10.1021/nl034946t.
[102] A.V. Krasheninnikov, K. Nordlund, J. Keinonen, F. Banhart, Ion-irradiation-induced welding of carbon nanotubes, Phys. Rev. B 66 (2002) 245403, http://dx.doi.org/10.1103/PhysRevB.66.245403.
[103] H.W.C. Postma, M. de Jonge, Z. Yao, C. Dekker, Electrical transport through carbon nanotube junctions created by mechanical manipulation, Phys. Rev. B 62 (2000) R10653–R10656, http://dx.doi.org/10.1103/PhysRevB.62.R10653.
[104] P.W. Chiu, G.S. Duesberg, U. Dettlaff-Weglikowska, S. Roth, Interconnection of carbon nanotubes by chemical functionalization, Appl. Phys. Lett. 80 (20) (2002) 3811–3813, http://dx.doi.org/10.1063/1.1480487.
[105] F.Y. Meng, S.Q. Shi, D.S. Xu, R. Yang, Multiterminal junctions formed by heating ultrathin single-walled carbon nanotubes, Phys. Rev. B 70 (2004) 125418, http://dx.doi.org/10.1103/PhysRevB.70.125418.
[106] A. Cummings, M. Osman, D. Srivastava, M. Menon, Thermal conductivity of Y-junction carbon nanotubes, Phys. Rev. B 70 (2004) 115405, http://dx.doi.org/10.1103/PhysRevB.70.115405.
[107] C. Ren, Z. Xu, W. Zhang, Y. Li, Z. Zhu, P. Huai, Theoretical study of heat conduction in carbon nanotube hetero-junctions, Phys. Lett. A 374 (17) (2010) 1860–1865, http://dx.doi.org/10.1016/j.physleta.2010.02.028.
[108] R.S. Prasher, X.J. Hu, Y. Chalopin, N. Mingo, K. Lofgreen, S. Volz, F. Cleri, P. Keblinski, Turning carbon nanotubes from exceptional heat conductors into insulators, Phys. Rev. Lett. 102 (2009) 105901, http://dx.doi.org/10.1103/PhysRevLett.102.105901.
[109] K.J. Zhang, A. Yadav, K.H. Kim, Y. Oh, M.F. Islam, C. Uher, K.P. Pipe, Thermal and electrical transport in ultralow density single-walled carbon nanotube networks, Adv. Mater. 25 (21) (2013) 2926–2931, http://dx.doi.org/10.1002/adma.201300059.
[110] V. Varshney, A.K. Roy, G. Froudakis, B.L. Farmer, Molecular dynamics simulations of thermal transport in porous nanotube network structures, Nanoscale 3 (2011) 3679–3684, http://dx.doi.org/10.1039/C1NR10331H.
[111] J. Chen, X. Gui, Z. Wang, Z. Li, R. Xiang, K. Wang, D. Wu, X. Xia, Y. Zhou, Q. Wang, Z. Tang, L. Chen, Superlow thermal conductivity 3D carbon nanotube network for thermoelectric applications, ACS Appl. Mater. Interfaces 4 (1) (2012) 81–86, http://dx.doi.org/10.1021/am201330f.
[112] Q. Kong, L. Qiu, Y.D. Lim, C.W. Tan, K. Liang, C. Lu, B.K. Tay, Thermal conductivity characterization of three dimensional carbon nanotube network using freestanding sensor-based 3ω technique, Surf. Coat. Technol. 345 (2018) 105–112, http://dx.doi.org/10.1016/j.surfcoat.2018.03.090.
[113] M.K. Samani, C. Lu, Q. Kong, N. Khosravian, G. Chen, C.W. Tan, P. Rudquist, B.K. Tay, J. Liu, Thermal conductivity enhancement of carbon@ carbon nanotube arrays and bonded carbon nanotube network, Mater. Res. Express 6 (8) (2019) 085616, http://dx.doi.org/10.1088/2053-1591/ab1e60.
[114] A.N. Volkov, L.V. Zhigilei, Scaling laws and mesoscopic modeling of thermal conductivity in carbon nanotube materials, Phys. Rev. Lett. 104 (21) (2010) 215902, http://dx.doi.org/10.1103/PhysRevLett.104.215902.
[115] Y. Yue, X. Huang, X. Wang, Thermal transport in multiwall carbon nanotube buckypapers, Phys. Lett. A 374 (40) (2010) 4144–4151, http://dx.doi.org/10.1016/j.physleta.2010.08.034.
[116] P. Gonnet, Z. Liang, E.S. Choi, R.S. Kadambala, C. Zhang, J.S. Brooks, B. Wang, L. Kramer, Thermal conductivity of magnetically aligned carbon nanotube buckypapers and nanocomposites, Curr. Appl. Phys. 6 (1) (2006) 119–122, http://dx.doi.org/10.1016/j.cap.2005.01.053.
[117] M.B. Jakubinek, M.A. White, G. Li, C. Jayasinghe, W. Cho, M.J. Schulz, V. Shanov, Thermal and electrical conductivity of tall, vertically aligned carbon nanotube arrays, Carbon 48 (13) (2010) 3947–3952, http://dx.doi.org/10.1016/j.carbon.2010.06.063.
[118] B.A. Cola, J. Xu, C. Cheng, X. Xu, T.S. Fisher, H. Hu, Photoacoustic characterization of carbon nanotube array thermal interfaces, J. Appl. Phys. 101 (5) (2007) 054313, http://dx.doi.org/10.1063/1.2510998.
[119] M.L. Bauer, Q.N. Pham, C.B. Saltonstall, P.M. Norris, Thermal conductivity of vertically aligned carbon nanotube arrays: Growth conditions and tube inhomogeneity, Appl. Phys. Lett. 105 (15) (2014) 151909, http://dx.doi.org/10.1063/1.4898708.
[120] M.O. Memon, S. Haillot, K. Lafdi, Carbon nanofiber based buckypaper used as a thermal interface material, Carbon 49 (12) (2011) 3820–3828, http://dx.doi.org/10.1016/j.carbon.2011.05.015.

[121] Y. Yue, K. Liu, M. Li, X. Hu, Thermal manipulation of carbon nanotube fiber by mechanical stretching, Carbon 77 (2014) 973–979, http://dx.doi.org/10.1016/j.carbon.2014.06.013.
[122] T. Zhou, Y. Niu, Z. Li, H. Li, Z. Yong, K. Wu, Y. Zhang, Q. Li, The synergetic relationship between the length and orientation of carbon nanotubes in direct spinning of high-strength carbon nanotube fibers, Mater. Des. 203 (2021) 109557, http://dx.doi.org/10.1016/j.matdes.2021.109557.
[123] M. Lee, Y.H. Kang, J. Kim, Y.K. Lee, S.Y. Cho, Freely shapable and 3D porous carbon nanotube foam using rapid solvent evaporation method for flexible thermoelectric power generators, Adv. Energy Mater. 9 (29) (2019) 1900914, http://dx.doi.org/10.1002/aenm.201900914.
[124] M. Statz, S. Schneider, F.J. Berger, L. Lai, W.A. Wood, M. Abdi-Jalebi, S. Leingang, H.-J. Himmel, J. Zaumseil, H. Sirringhaus, Charge and thermoelectric transport in polymer-sorted semiconducting single-walled carbon nanotube networks, ACS Nano 14 (11) (2020) 15552–15565, http://dx.doi.org/10.1021/acsnano.0c06181.
[125] M.S. Dresselhaus, G. Dresselhaus, R. Saito, A. Jorio, Raman spectroscopy of carbon nanotubes, Phys. Rep. 409 (2) (2005) 47–99, http://dx.doi.org/10.1016/j.physrep.2004.10.006.
[126] J.-H. Kim, A. Nugraha, L. Booshehri, E. Hároz, K. Sato, G. Sanders, K.-J. Yee, Y.-S. Lim, C. Stanton, R. Saito, J. Kono, Coherent phonons in carbon nanotubes and graphene, Chem. Phys. 413 (2013) 55–80, http://dx.doi.org/10.1016/j.chemphys.2012.09.017.
[127] J. Chen, J. He, D. Pan, X. Wang, N. Yang, J. Zhu, S.A. Yang, G. Zhang, Emerging theory and phenomena in thermal conduction: A selective review, Sci. China Phys. Mech. 65 (11) (2022) 117002, http://dx.doi.org/10.1007/s11433-022-1952-3.
[128] R. Anufriev, J. Maire, M. Nomura, Review of coherent phonon and heat transport control in one-dimensional phononic crystals at nanoscale, APL Mater. 9 (7) (2021) 070701, http://dx.doi.org/10.1063/5.0052230.
[129] A. Gambetta, C. Manzoni, E. Menna, M. Meneghetti, G. Cerullo, G. Lanzani, S. Tretiak, A. Piryatinski, A. Saxena, R.L. Martin, A.R. Bishop, Real-time observation of nonlinear coherent phonon dynamics in single-walled carbon nanotubes, Nat. Phys. 2 (8) (2006) 515–520, http://dx.doi.org/10.1038/nphys345.
[130] M. Hada, K. Makino, H. Inoue, T. Hasegawa, H. Masuda, H. Suzuki, K. Shirasu, T. Nakagawa, T. Seki, J. Matsuo, T. Nishikawa, Y. Yamashita, S. Koshihara, V. Stolojan, S.R.P. Silva, J. Fujita, Y. Hayashi, S. Maeda, M. Hase, Phonon transport probed at carbon nanotube yarn/sheet boundaries by ultrafast structural dynamics, Carbon 170 (2020) 165–173, http://dx.doi.org/10.1016/j.carbon.2020.08.026.
[131] C. Köhler, T. Watermann, E. Malic, Time- and momentum-resolved phonon-induced relaxation dynamics in carbon nanotubes, J. Phys.: Condens. Matter 25 (10) (2013) 105301, http://dx.doi.org/10.1088/0953-8984/25/10/105301.
[132] L. Chen, S. Kumar, Thermal transport in double-wall carbon nanotubes using heat pulse, J. Appl. Phys. 110 (7) (2011) 074305, http://dx.doi.org/10.1063/1.3641970.
[133] S. Kumar, J.Y. Murthy, Interfacial thermal transport between nanotubes, J. Appl. Phys. 106 (8) (2009) 084302, http://dx.doi.org/10.1063/1.3245388.
[134] E. Ghavaminezhad, M. Mahnama, N. Zolfaghari, The effects of van der waals interactions on the vibrational behavior of single-walled carbon nanotubes using the hammer impact test: a molecular dynamics study, Phys. Chem. Chem. Phys. 22 (2020) 12613–12623, http://dx.doi.org/10.1039/D0CP00856G.
[135] X.H. Zhang, G.E. Santoro, U. Tartaglino, E. Tosatti, Dynamical chiral symmetry breaking in sliding nanotubes, Phys. Rev. Lett. 102 (2009) 125502, http://dx.doi.org/10.1103/PhysRevLett.102.125502.
[136] M.V.D. Prasad, B. Bhattacharya, Phononic origins of friction in carbon nanotube oscillators, Nano Lett. 17 (4) (2017) 2131–2137, http://dx.doi.org/10.1021/acs.nanolett.6b04310.
[137] Q.J. Wang, J.G. Che, Origins of distinctly different behaviors of Pd and Pt contacts on graphene, Phys. Rev. Lett. 103 (2009) 066802, http://dx.doi.org/10.1103/PhysRevLett.103.066802.
[138] J. Xu, Y. He, Thermal analysis of NR composite with MWCNTs aligned in a magnetic field, Int. J. Polym. Sci. 2015 (2015) 305317, http://dx.doi.org/10.1155/2015/305317.
[139] J. Wang, H. Xie, Z. Xin, Y. Li, Increasing the thermal conductivity of palmitic acid by the addition of carbon nanotubes, Carbon 48 (14) (2010) 3979–3986, http://dx.doi.org/10.1016/j.carbon.2010.06.044.
[140] Y. Li, H. Zhang, Y. Chen, Z. Shi, X. Cao, Z. Guo, P.K. Shen, Nitrogen-doped carbon-encapsulated SnO_2@Sn nanoparticles uniformly grafted on three-dimensional graphene-like networks as anode for high-performance lithium-ion batteries, ACS Appl. Mater. Interfaces 8 (1) (2016) 197–207, http://dx.doi.org/10.1021/acsami.5b08340.
[141] L. Qiu, H. Zou, X. Wang, Y. Feng, X. Zhang, J. Zhao, X. Zhang, Q. Li, Enhancing the interfacial interaction of carbon nanotubes fibers by au nanoparticles with improved performance of the electrical and thermal conductivity, Carbon 141 (2019) 497–505, http://dx.doi.org/10.1016/j.carbon.2018.09.073.
[142] D. Suh, C.M. Moon, D. Kim, S. Baik, Ultrahigh thermal conductivity of interface materials by silver-functionalized carbon nanotube phonon conduits, Adv. Mater. 28 (33) (2016) 7220–7227, http://dx.doi.org/10.1002/adma.201600642.
[143] T.S. Gspann, S.M. Juckes, J.F. Niven, M.B. Johnson, J.A. Elliott, M.A. White, A.H. Windle, High thermal conductivities of carbon nanotube films and micro-fibres and their dependence on morphology, Carbon 114 (2017) 160–168, http://dx.doi.org/10.1016/j.carbon.2016.12.006.
[144] L. Qiu, F. Li, N. Zhu, Y. Feng, X. Zhang, X. Zhang, Broad low-frequency phonon resonance for increased across-tube heat transport, Phys. Rev. B 105 (2022) 165406, http://dx.doi.org/10.1103/PhysRevB.105.165406.
[145] L. Qiu, F. Li, N. Zhu, Y. Feng, X. Zhang, X. Zhang, Elaborate manipulation on CNT intertube heat transport by using a polymer knob, Int. J. Heat Mass Transfer 184 (2022) 122280, http://dx.doi.org/10.1016/j.ijheatmasstransfer.2021.122280.
[146] A. Badakhsh, Y. Lee, K.Y. Rhee, C.W. Park, K. An, B. Kim, Improvement of thermal, electrical and mechanical properties of composites using a synergistic network of length controlled-CNTs and graphene nanoplatelets, Composites B 175 (2019) 107075, http://dx.doi.org/10.1016/j.compositesb.2019.107075.
[147] M. Safdari, M.S. AlHaik, Synergistic electrical and thermal transport properties of hybrid polymeric nanocomposites based on carbon nanotubes and graphite nanoplatelets, Carbon 64 (2013) 111–121, http://dx.doi.org/10.1016/j.carbon.2013.07.042.
[148] Y. Xiao, W. Wang, X. Chen, T. Lin, Y. Zhang, J. Yang, Y. Wang, Z. Zhou, Hybrid network structure and thermal conductive properties in poly(vinylidene fluoride) composites based on carbon nanotubes and graphene nanoplatelets, Composites A 90 (2016) 614–625, http://dx.doi.org/10.1016/j.compositesa.2016.08.029.
[149] J. Yu, H.K. Choi, H.S. Kim, S.Y. Kim, Synergistic effect of hybrid graphene nanoplatelet and multi-walled carbon nanotube fillers on the thermal conductivity of polymer composites and theoretical modeling of the synergistic effect, Composites A 88 (2016) 79–85, http://dx.doi.org/10.1016/j.compositesa.2016.05.022.
[150] Y. Guo, C. Cao, F. Luo, B. Huang, L. Xiao, Q. Qian, Q. Chen, Largely enhanced thermal conductivity and thermal stability of ultra high molecular weight polyethylene composites via BN/CNT synergy, RSC Adv. 9 (2019) 40800–40809, http://dx.doi.org/10.1039/C9RA08416A.
[151] J. Che, K. Wu, Y. Lin, K. Wang, Q. Fu, Largely improved thermal conductivity of HDPE/expanded graphite/carbon nanotubes ternary composites via filler network-network synergy, Composites A 99 (2017) 32–40, http://dx.doi.org/10.1016/j.compositesa.2017.04.001.
[152] J. Che, M. Jing, D. Liu, K. Wang, Q. Fu, Largely enhanced thermal conductivity of HDPE/boron nitride/carbon nanotubes ternary composites via filler network-network synergy and orientation, Composites A 112 (2018) 32–39, http://dx.doi.org/10.1016/j.compositesa.2018.05.016.
[153] C. Ji, C. Yan, Y. Wang, S. Xiong, F. Zhou, Y. Li, R. Sun, C.-P. Wong, Thermal conductivity enhancement of CNT/MoS_2/graphene–epoxy nanocomposites based on structural synergistic effects and interpenetrating network, Composites B 163 (2019) 363–370, http://dx.doi.org/10.1016/j.compositesb.2018.11.005.
[154] P. Szatkowski, K. Pielichowska, S. Blazewicz, Mechanical and thermal properties of carbon-nanotube-reinforced self-healing polyurethanes, J. Mater. Sci. 52 (20) (2017) 12221–12234, http://dx.doi.org/10.1007/s10853-017-1353-6.
[155] H. Yu, Y. Feng, C. Chen, Z. Zhang, Y. Cai, M. Qin, W. Feng, Thermally conductive, self-healing, and elastic polyimide@vertically aligned carbon nanotubes composite as smart thermal interface material, Carbon 179 (2021) 348–357, http://dx.doi.org/10.1016/j.carbon.2021.04.055.
[156] M. Shen, W.J. Evans, D. Cahill, P. Keblinski, Bonding and pressure-tunable interfacial thermal conductance, Phys. Rev. B 84 (2011) 195432, http://dx.doi.org/10.1103/PhysRevB.84.195432.
[157] M. Hu, P. Keblinski, J.-S. Wang, N. Raravikar, Interfacial thermal conductance between silicon and a vertical carbon nanotube, J. Appl. Phys. 104 (8) (2008) 083503, http://dx.doi.org/10.1063/1.3000441.
[158] J. Chen, J.H. Walther, P. Koumoutsakos, Covalently bonded graphene–carbon nanotube hybrid for high-performance thermal interfaces, Adv. Funct. Mater. 25 (48) (2015) 7539–7545, http://dx.doi.org/10.1002/adfm.201501593.
[159] Y. Ni, H. Le Khanh, Y. Chalopin, J. Bai, P. Lebarny, L. Divay, S. Volz, Highly efficient thermal glue for carbon nanotubes based on azide polymers, Appl. Phys. Lett. 100 (19) (2012) 193118, http://dx.doi.org/10.1063/1.4711809.
[160] R. Cross, B.A. Cola, T. Fisher, X. Xu, K. Gall, S. Graham, A metallization and bonding approach for high performance carbon nanotube thermal interface materials, Nanotechnology 21 (44) (2010) 445705, http://dx.doi.org/10.1088/0957-4484/21/44/445705.
[161] L. Qiu, P. Guo, Q. Kong, C.W. Tan, K. Liang, J. Wei, J.N. Tey, Y. Feng, X. Zhang, B.K. Tay, Coating-boosted interfacial thermal transport for carbon nanotube array nano-thermal interface materials, Carbon 145 (2019) 725–733, http://dx.doi.org/10.1016/j.carbon.2019.01.085.
[162] M.A. Peacock, C.K. Roy, M.C. Hamilton, R. Wayne Johnson, R.W. Knight, D.K. Harris, Characterization of transferred vertically aligned carbon nanotubes arrays as thermal interface materials, Int. J. Heat Mass Transfer 97 (2016) 94–100, http://dx.doi.org/10.1016/j.ijheatmasstransfer.2016.01.071.
[163] Y. Wu, C.H. Liu, H. Huang, S.S. Fan, Effects of surface metal layer on the thermal contact resistance of carbon nanotube arrays, Appl. Phys. Lett. 87 (21) (2005) 213108, http://dx.doi.org/10.1063/1.2133916.

[164] L. Ping, P.-X. Hou, C. Liu, J. Li, Y. Zhao, F. Zhang, C. Ma, K. Tai, H. Cong, H.-M. Cheng, Surface-restrained growth of vertically aligned carbon nanotube arrays with excellent thermal transport performance, Nanoscale 9 (2017) 8213–8219, http://dx.doi.org/10.1039/C7NR01529A.

[165] L. Qiu, X. Wang, G. Su, D. Tang, X. Zheng, J. Zhu, Z. Wang, P.M. Norris, P.D. Bradford, Y. Zhu, Remarkably enhanced thermal transport based on a flexible horizontally-aligned carbon nanotube array film, Sci. Rep. 6 (2016) 21014, http://dx.doi.org/10.1038/srep21014.

[166] M.T. Barako, Y. Gao, Y. Won, A.M. Marconnet, M. Asheghi, K.E. Goodson, Reactive metal bonding of carbon nanotube arrays for thermal interface applications, IEEE Trans. Compon. Pack. Manuf. Technol. 4 (12) (2014) 1906–1913, http://dx.doi.org/10.1109/TCPMT.2014.2369371.

[167] L. Qiu, K. Scheider, S.A. Radwan, L.S. Larkin, C.B. Saltonstall, Y. Feng, X. Zhang, P.M. Norris, Thermal transport barrier in carbon nanotube array nano-thermal interface materials, Carbon 120 (2017) 128–136, http://dx.doi.org/10.1016/j.carbon.2017.05.037.